University of Thessaly – School of Natural Sciences

Department of Physics

Investigation of Biosignatures in Mimic Soils and Lunar Dust after exposure to high-energy radiation (UV, X-rays, Lasers)

Ioannis Theiakoulis

itheiakoulis@uth.gr

Undergraduate student

Undergraduate Thesis

Submitted to meet part of the requirements for obtaining the degree in Physics

Lamia – Spring Semester 2024–2025

Approved by the Members of the three-member Examination Committee

First Examiner (Supervisor): *Nikolaos Petropoulos*
Assistant Professor, Department of Physics, University of Thessaly

Second Examiner (Supervisor): *Elias Chatzitheodoridis*
Professor, School of Mining and Metallurgical Engineering, NTUA

Third Examiner: *Athanasios Kanapitsas*
Professor, Department of Physics, University of Thessaly

Acknowledgments

I wish to express my sincere gratitude to my thesis advisors, Professor Elias Chatzitheodoridis and Assistant Professor Nikolaos Petropoulos, for their invaluable guidance, support, and expertise throughout the course of this research. Their thoughtful feedback, encouragement, and continuous availability have been essential to the successful completion of this work, and I am deeply indebted to them for the opportunity to conduct this thesis under their supervision.

I would also like to thank the members of the examination committee for their careful evaluation of this work and for their constructive suggestions, which have significantly contributed to its improvement.

My appreciation is further extended to the faculty and staff of the Department of Physics at the University of Thessaly, whose teaching, assistance, and resources have played a central role in shaping my academic development.

Finally, I am profoundly grateful to my family and friends for their unwavering patience, encouragement, and support. Their belief in me has been a source of strength throughout this endeavor.

This thesis is dedicated to the exploration of space, a passion that has continually inspired and guided me during the course of my studies.

Ioannis Theiakoulis

Διερεύνηση βιοϋπογραφών σε μιμητικά εδάφη και σεληνιακή σκόνη μετά από επίδραση ισχυρής ακτινοβολίας (UV, Xrays, Lasers)

Ιωάννης Θειακούλης
Πανεπιστήμιο Θεσσαλίας, Τμήμα Φυσικής, Ιανουάριος 2025

Επιβλέπων Καθηγητής: Νικόλαος Πετρόπουλος – Επίκουρος Καθηγητής

Περίληψη

Η αναζήτηση ζωής πέρα από τη Γη, που αποτελεί θεμέλιο της αστροβιολογίας, συνιστά μία από τις πιο φιλόδοξες και διεπιστημονικές επιστημονικές επιδιώξεις της σύγχρονης εποχής. Με την πρόοδο των διαστημικών αποστολών και την επέκταση της ανθρώπινης παρουσίας στο Διάστημα, καθίσταται επιτακτική η μελέτη των ορίων επιβίωσης της ζωής υπό ακραίες εξωγήινες συνθήκες. Η παρούσα διπλωματική εργασία διερευνά την ανθεκτικότητα του εξτρεμόφιλου μύκητα Ulocladium chartarum όταν εκτίθεται ταυτόχρονα σε δύο κρίσιμους παράγοντες: τη σεληνιακή σκόνη και την ακτινοβολία υψηλής ενέργειας. Οι συνθήκες αυτές προσομοιώνουν το σκληρό επιφανειακό περιβάλλον της Σελήνης και άλλων ατμοσφαιρικά απογυμνωμένων ουράνιων σωμάτων.

Ο πειραματικός σχεδιασμός περιλάμβανε την καλλιέργεια του Ulocladium chartarum σε θρεπτικά μέσα και την έκθεσή του σε προσομοιωμένη σεληνιακή σκόνη (μέσω λέιζερ) και παράλληλα σε υπεριώδη ακτινοβολία UV-C, ακτίνες X και παλμική ακτινοβολία λέιζερ. Ομάδα ελέγχου χωρίς έκθεση σε σκόνη λειτούργησε ως σημείο σύγκρισης. Τα αποτελέσματα αποκάλυψαν αξιοσημείωτη ανθεκτικότητα του μύκητα, με εντοπισμένες μεταβολές στη μορφολογία και την χρωστική του, υποδηλώνοντας την ύπαρξη ισχυρών βιοχημικών και δομικών μηχανισμών αντίστασης. Η σεληνιακή σκόνη ενίσχυσε το οξειδωτικό στρες και επηρέασε δυσμενώς τη θρέψη και την ανάπτυξη του οργανισμού, υποδεικνύοντας τοξικό δυναμικό και φυσικοχημική παρεμβολή.

Παράλληλα, αναπτύχθηκε και υλοποιήθηκε ένα προηγμένο υπολογιστικό σύστημα αυτοματοποίησης, το οποίο συνδύασε καταγραφή δεδομένων (θερμοκρασία, υγρασία, ένταση φωτός, πίεση) με χρονομετρημένη απεικόνιση και αλγορίθμους τεχνητής νοημοσύνης (AI) για την πρόβλεψη περιβαλλοντικών μεταβολών. Η εν λόγω πλατφόρμα συνέβαλε στη σταθερότητα του πειράματος και στην αξιόπιστη προσομοίωση εξωγήινων περιβαλλόντων, ενώ επιτρέπει την κλιμάκωση σε μελλοντικά διαστημικά πειράματα μακράς διάρκειας.

Επιπλέον, η εργασία διερευνά την πιθανότητα σχηματισμού βιοϋπογραφών υπό τέτοιες συνθήκες. Αν και δεν καταγράφηκαν σαφείς μοριακές ενδείξεις ζωής, οι μορφολογικές και χρωστικές μεταβολές που παρατηρήθηκαν θα μπορούσαν να λειτουργήσουν ως δευτερεύοντες δείκτες βιολογικής δραστηριότητας, επισημαίνοντας την ανάγκη για πολυδιάστατες μεθόδους ανίχνευσης ζωής που να συνδυάζουν φασματοσκοπία, απεικόνιση και υπολογιστική ανάλυση.

Η εργασία αυτή ενισχύει την επιστημονική κατανόηση της μικροβιακής επιβίωσης σε συνθήκες διαστήματος και προσφέρει ένα νέο πρότυπο για αστροβιολογικά πειράματα, συνδυάζοντας βιολογική παρατήρηση με τεχνολογικά καινοτόμες μεθόδους. Τα ευρήματα έχουν εφαρμογή σε διαστημικές αποστολές όπως το πρόγραμμα Artemis της NASA και μελλοντικές αποστολές στον Άρη, ενώ υποστηρίζουν την ανάπτυξη αυτοματοποιημένων πειραματικών πλατφορμών με στόχο την ανίχνευση ζωής σε άλλους πλανήτες.

Λέξεις Κλειδιά: *Ulocladium chartarum, Σεληνιακή Σκόνη, Ακτινοβολία Υψηλής Ενέργειας, Αστροβιολογία, Βιοϋπογραφές, Μικροβιακή Ανθεκτικότητα, Τεχνητή Νοημοσύνη, Εξωγήινα Περιβάλλοντα, Διαστημική Βιολογία, Πλανητική Εξερεύνηση*

Investigation of Biosignatures in Mimic Soils and Lunar Dust after exposure to high-energy radiation (UV, X-rays, Lasers)

Ioannis Thiakoules
University of Thessaly, Physics Department, January 2025

Supervisor: Nicholas Petropoulos – Assistant Professor

Abstract

The search for life beyond Earth—central to the field of astrobiology—remains one of the most profound scientific frontiers of the modern era. As space exploration advances, defining the biological limits of life in extraterrestrial environments becomes increasingly critical. This thesis intends to set the tools to investigate the resilience of the extremotolerant fungus Ulocladium chartarum under dual cosmic stressors: simulated lunar dust and high-energy radiation. These conditions emulate the hostile surface environments of airless celestial bodies such as the Moon, where intense radiation and reactive regolith present both biological and engineering challenges.

The experimental design involved cultivating U. chartarum on agar plates and exposing it to laser-ablated lunar regolith simulants in combination with UV-C, X-ray, and pulsed laser radiation. A control cohort, maintained under identical conditions without regolith exposure, enabled differential analysis. Preliminary observations of the colonies of fungi developed in Petri dishes revealed notable persistence of fungals, characterized by continued growth, altered hyphal morphology, and potential stress-induced pigmentation. Lunar dust exacerbated oxidative stress and appeared to disrupt nutrient dynamics, further modulating the organism's physiological response. These findings offer key insights into the biochemical and structural mechanisms by which microorganisms may withstand—and adapt to—radiation-saturated extraterrestrial environments.

In parallel, a custom computational system was developed to automate environmental monitoring and data acquisition. The platform integrated time-lapse imaging, multiparameter sensing (temperature, humidity, light intensity, and pressure), and predictive modeling via artificial intelligence. This system enabled high-resolution, real-time feedback loops for environmental control and established a reproducible

framework for long-duration space biology experiments. The integration of biological exposure studies with computational foresight represents a methodological advance, enabling precision experimentation under astrobiological constraints.

The study also examined the potential for biosignature formation under such conditions. While definitive biosignatures were not detected, observed morphological and pigmentary changes constitute plausible proxies of biological activity that warrant further spectroscopic and biochemical characterization. These results highlight the importance of multidimensional biosignature detection strategies that combine structural, chemical, and temporal indicators.

This thesis contributes both empirically and methodologically to the field of astrobiology. It advances understanding of extremophilic survival strategies, informs planetary protection protocols, and provides a scalable experimental model for extraterrestrial life detection. The findings bear particular relevance to forthcoming missions, including NASA's Artemis program and future crewed or robotic expeditions to the Moon and Mars. By integrating experimental microbiology with autonomous computational platforms, this work lays the foundation for more sophisticated systems capable of probing the biological limits of life beyond Earth.

Keywords: *Ulocladium chartarum, Lunar Regolith, High-Energy Radiation, Astrobiology, Biosignatures, Microbial Resilience, Artificial Intelligence, Space Biology, Extraterrestrial Environments, Planetary Exploration*

Contents

Chapter 1

Introduction

The quest for detecting extraterrestrial life is intrinsically linked to our understanding of how life responds to the extreme conditions of space. Extremophilic organisms that thrive in harsh environments provide crucial insight into this endeavor. Among them, fungi such as Ulocladium Chartarum demonstrate remarkable resilience, making them candidates for studying the preservation of biosignatures and the resistance of microorganisms under simulated extraterrestrial conditions. To conduct laboratory experiments, analogs of lunar regolith and terrains that mimic lunar dust were used, replicating the properties of the lunar surface. These analogs are vital for both biosignature studies and the calibration of instruments designed for planetary missions.

Soil analogues have been designed to replicate the diverse compositions of the topography of various planets. In the case of Mars analogs, the mimetic soil replicates the iron-rich basaltic composition of the Martian regolith and includes a mixture of silicates, oxides, and sulfate salts. Regarding lunar dust analogs, such as NU-LHT-2M and NU-LHT-2C, they simulate the mineralogy of lunar mountainous regions and mare areas, respectively.

Biosignatures are indicators of past or present life that encompass a wide spectrum of chemical, physical, and morphological characteristics. The detection of biosignatures is crucial for missions such as the Mars Science Laboratory (Curiosity Rover), ExoMars, and Artemis lunar missions. The precise interpretation of potential biosignatures is of paramount importance for understanding the history of life in the Solar System.

Biosignatures can be categorized into various classes:

1. Organic Molecules: These include amino acids, nucleic acids, lipids, and complex organic compounds, which are the fundamental building blocks of life.

2. Isotopic Patterns: Life tends to favor certain isotopes, leading to distinctive isotopic ratios that can signal biological processes.

3. Morphological Characteristics: Structures such as microbial mats, stromatolites, and microfossils provide physical evidence of life.

4. Biominerals: Minerals precipitated by biological activity, such as magnetite or carbonate structures, are indicative of biological processes.

This study establishes the methodological framework for examining the effects of high-energy radiation—including ultraviolet (UV), X-rays, and laser irradiation—on biosignatures in simulated soils and lunar dust. Each of these radiation types can significantly modify the chemical and physical properties of materials, thereby influencing the stability and detectability of potential biosignatures. In the context of astrobiology, such investigations are critical, as planetary surfaces lacking protective atmospheres expose organisms and biomolecules to intense radiation. This thesis discusses in detail the mechanisms by which high-energy radiation interacts with biosignatures and the implications of these interactions for their preservation and detection in extraterrestrial environments.

1.1 UV Radiation

Ultraviolet (UV) radiation is classified into three categories: UVA (315 - 400 nm), UVB (280 - 315 nm), and UVC (200 - 280 nm). UVC radiation, in particular, contains high-energy photons capable of breaking chemical bonds and initiating photochemical reactions. On planetary surfaces, such as that of Mars, UV radiation plays a significant role due to the planet's thin atmosphere and lack of a magnetic field. Studies have shown that UV radiation can lead to the degradation of organic molecules, thereby affecting their detectability.

Research by Guan et al. found that prolonged exposure to ultraviolet radiation resulted in the photolysis of amino acids, leading to the formation of simpler organic compounds and free radicals. The extent of degradation was influenced by factors such as the initial concentration of organic molecules and the presence of mineral matrices that could offer some protective effects. Experiments exposing soil analogs and lunar dust to UV radiation typically employ sources such as deuterium or mercury lamps to simulate solar UV radiation or alteration of biosignatures.

UV radiation primarily induces the breaking of chemical bonds, leading to the formation of radicals and other reactive species. Amino acids, nucleic acids, and lipids are particularly sensitive to photodegradation. Studies have demonstrated that amino acids like glycine and alanine decompose into simpler molecules such as formaldehyde and ammonia upon exposure to UV radiation.

Despite the destructive potential of UV radiation, mineral matrices such as clays and sulfate salts have been shown to provide some protection to organic molecules from radiation-induced damaged. Bishop et al. , observed that clay could protect amino acids from UV-induced degradation. Mineral matrices can absorb organic molecules onto their surfaces, offering a natural shield that reduces their exposure to radiation. Therefore, the long-term preservation of biosignatures in extraterrestrial environments depends on factors such as the stability of mineral matrices, environmental conditions, and the intensity and duration of radiation exposure. The aforementioned study demonstrated that certain organic molecules could remain stable for extended periods if adequately protected by mineral matrices.

1.2 X-rays

X-rays are characterized by high energy and the ability to penetrate deeper into materials compared to UV radiation. They are representative of cosmic radiation and solar rays that impact planetary sufaces. Exposure to X-rays can induce radiolysis, resulting in the formation of reactive oxygen species (ROS) and other radicals capable of degrading organic molecules. Understanding the effects of X-rays is crucial for interpreting data from surface and subsurface analyses on planetary bodies.

X-rays can penetrate deeper into materials than UV radiation, causing more extensive radiolytic degradation. The interaction of X-ray radiation on amino acids led to the formation of oxidized products, such as carboxylic acids and aldehydes.

1.3 Lasers

Lasers provide coherent, high-intensity light that can simulate various extraterrestrial processes, including micrometeoroid impacts and focused solar energy. Laser-induced breakdown spectroscopy (LIBS) and Raman spectroscopy are commonly used in these studies to analyze the chemical and structural changes in samples after laser irradiation.

The ability of lasers to cause thermal and mechanical damage makes them a valuable tool for simulating extraterrestrial conditions. In the mentioned study, LIBS was used to analyze laser-irradiated samples, and the formation of microcraters and partial evaporation of surface materials was observed. The chemical composition of the evaporated material often differed from the original sample, highlighting the possibility of laser-induced alteration of biosignatures. Specifically, laser irradiation can cause local heating, leading to thermal decomposition and evaporation of organic molecules.

Mechanical effects include, in addition to microcrater formation, particle fragmentation.

The extent of thermal and mechanical damage depends on laser parameters, such as wavelength, pulse duration, and energy density. For lunar exploration, including the Artemis program, understanding the effects of high-energy radiation on potential biosignatures is crucial for probiotic chemical research. The results of laser radiation studies, in particular, are relevant to the use of laser-based instruments on lunar rovers.

Microorganisms, including bacteria, viruses, and fungi, are fundamental to all ecosystems as they play a crucial role in biogeochemical cycles and human health. Below, we will delve into the complex mechanisms that govern microbial resistance, with an emphasis on fungal resistance and an analysis of a fungus of major importance: Ulocladium chartarum.

Microorganisms ranging from bacteria to protozoa have various mechanisms that allow them to survive and multiply despite the presence of antimicrobial agents. Antimicrobial resistance (AMR) includes a variety of mechanisms, which are examined in detail below:

One of the main mechanisms of resistance in bacteria is the production of enzymes that degrade or modify antimicrobial agents. For example, some enzymes can break down complex organic molecules, making them less toxic and manageable for the microorganism. The kinetic energy of enzymatic degradation can be described using the Michaelis-Menten equations:

$$\Sigma E = \frac{\Sigma E_{\text{MAX}}[S]}{[S] + \kappa_M} \, , \tag{1.3.1}$$

where ΣE is the reaction rate, ΣE_{MAX} is the maximum rate achieved by the system, $[S]$ is the substrate concentration, and κ_M is the Michaelis constant. In the context of fungi, enzymes such as echinocandin-degrading enzymes can similarly inactivate antifungal agents.

The next mechanism is the efflux pumps, i.e., transport proteins involved in the elimination of toxic substances. These pumps can be classified into several large families, such as ATP-binding cassette (ABC) transporters and major facilitator superfamily (MFS) transporters.

The mathematical modeling of the kinetic energy of the efflux pump is expressed differentially by the following relationship:

$$\frac{\delta[\Delta\varepsilon_{\nu\theta}]}{dt} = -[\Delta\varepsilon_{\nu\theta}] \cdot \kappa \, , \tag{1.3.2}$$

where [Δ] is the intracellular concentration of the substance and κ is the efflux rate constant.

In addition, microorganisms can develop resistance by modifying the targets of antimicrobial agents. For example, mutations in specific genes can change the structure of target proteins, reducing the binding affinity of toxicants. The equation can describe the impact of target modification on substance binding:

$$\kappa_{\rho\varepsilon} = \frac{[A] \cdot [B]}{[AB]} \ , \tag{1.3.3}$$

where $\kappa_{\rho\varepsilon}$ is the dissociation constant, $[A]$ and $[B]$ are the concentrations of the agent and target, respectively, and $[AB]$ is the concentration of the agent-target complex.

In fungi, target modifications often involve mutations in genes encoding key enzymes, affecting their interaction with potential inhibitors.

Biofilms are structured communities of microorganisms enclosed in a self-produced extracellular matrix that adheres to surfaces. Biofilm formation provides a protective environment that enhances resistance to environmental stresses and toxicants. Biofilm formation and growth can be modeled using logistic growth equations:

$$\frac{\delta B}{dt} = rB\left(1 - \frac{b}{k}\right) \ , \tag{1.3.4}$$

where b is the biomass of the biofilm, r is the intrinsic growth rate, and k is the carrying capacity of the environment.

Microbial resistance can evolve through mechanisms of genetic adaptation, including spontaneous mutations and horizontal gene transfer (HGT). HGT, facilitated by transformation, transduction, and conjugation, allows the rapid spread of resistance genes in microbial populations. The dynamics of gene transfer are represented as follows:

$$\frac{\delta \Sigma}{dt} = -\beta SI \ , \tag{1.3.5}$$

$$\frac{T}{dt} = \beta SI - \gamma I \ , \tag{1.3.6}$$

where S is the susceptible population, I is the resistant population, β is the rate of transmission, and γ is the rate of recovery or clearance.

The evolution of antimicrobial resistance is driven by selective pressures imposed by extreme environmental conditions. The basic reproductive number (R0), which indicates the average number of secondary transmissions produced by an infected individual, is a critical parameter.

$$R_0 = \frac{\beta N}{\gamma + \mu} \, , \tag{1.3.7}$$

where β is the transmission rate, N is the population density, γ is the recovery rate, and μ is the natural mortality rate.

Interventions aimed at reducing R0 below 1 are necessary to control the spread of resistance.

Of particular note are extremophiles, i.e. organisms that thrive in environments that are considered hostile or extreme. These environments include high or low temperatures, high radiation levels, extreme pH, high salinity, high pressure, and drought. Extremophiles are classified based on the type of extreme environment they inhabit. Some categories include thermophiles and hyperthermophiles, i.e. organisms that thrive in temperatures above 45 degrees Celsius. Next are the psychrophiles, the acidophiles, the alkalophiles, the halophiles, the barophiles, the xerophiles and finally the radiophiles. Radiophiles are also of particular importance in the present work, as they are organisms that thrive in environments with high levels of ionizing radiation, such as Deinococcus radiodurans.

One of the most peculiar mechanisms recorded by extremophile organisms is the DNA repair mechanism, i.e. the reassembly of their fragmented genome through precise repair processes. In addition, the survival of these organisms under high radiation conditions can be modeled using dose-response equations. It is valid,

$$S = S_0 \exp\left(-\frac{D}{D_{3.7}}\right) \, , \tag{1.3.8}$$

where S is the surviving fraction of microorganisms, S_0 is the initial population, D is the radiation dose, and $D_{3.7}$ is the dose required to reduce the population to 37% of its initial value.

This model helps to predict the survival rates of extremophiles exposed to cosmic radiation on planetary surfaces. Bacterial resistance mechanisms have been extensively studied due to their importance in various environments, including extreme habitats. Common mechanisms include enzymatic degradation, efflux pumps, and target modification.

In addition, bacteria exhibit sophisticated regulatory networks that coordinate these resistance mechanisms. Bacterial resistance is often regulated by complex networks that involve two-component systems. These networks allow bacteria to sense environmental cues and regulate resistance gene expression accordingly.

In the class of viruses, particularly those affecting extremophiles, resistance mechanisms emerge that allow their survival in hostile environments. Viral resistance often

arises through mutations in viral enzymes that target antiviral agents. For example, mutations in key viral genes can confer resistance to substances that would otherwise inhibit viral replication.

The high mutation rates of RNA viruses result in the formation of pseudotypes, which are dynamic populations of genetically diverse virions. The idea of pseudogenes is crucial to understanding viral resistance, as it allows the virus to adapt rapidly to selective pressures. Mathematically, the above is modeled as follows:

$$\Delta q = q(1-q)s \ , \tag{1.3.9}$$

where Δq is the change in the frequency of a resistant variant, q is its frequency, and s is the selection factor.

Protozoa are resistant to environmental pressures through mechanisms that include efflux pumps, target modification, and metabolic bypass. The genetic basis of resistance in protozoa often involves mutations in genes that encode critical proteins necessary for survival in extreme environments.

Mutational resistance in protozoa may bring about a change in physical condition, which affects the competitive ability of resistant strains in the absence of environmental pressures. The concept of fitness costs is essential for understanding the dynamic evolution of resistance and the possibility of resistance reversal. The above can be quantified as follows:

$$\Sigma E = \Sigma E_0 - \gamma R \ , \tag{1.3.10}$$

where ΣE is the fitness of the resistant strain, ΣE_0 is the fitness of the sensitive strain, γ is the fitness cost factor, and R is the resistance level.

Finally, fungi, a different group of eukaryotic organisms, include yeast, mold, and mushrooms. Adaptations of fungi to extreme environments and the emergence of resistance mechanisms provide important information for their possible survival on other planets.

Fungi use various mechanisms to resist environmental pressures, such as efflux pumps, target modification, biofilm formation, and pathways similar to those observed in bacteria, with great similarity in target modification and response pathways.

Efflux pumps in fungi, such as ATP-binding cassette transporters (ABCs) and carriers of the major facilitator superfamily (MFS), play a critical role in resistance by eliminating toxic substances from the cell. The kinetics of efflux pump action is identical to that described by equation (4.4). Overexpression of efflux pumps is a common mechanism of resistance in many fungal species.

Fungal biofilms are structured communities that exhibit enhanced resistance to environmental pressures and toxic substances. Biofilm formation includes the production of extracellular matrix components that prevent the penetration of harmful substances. The development of fungal biofilms is represented by equation (4.4). Fungi can activate response pathways to survive in extreme conditions. The thermal shock response and oxidative stress response pathways are examples of mechanisms that enhance fungal survival in extreme environments.

In this research paper, a study will be made of Ulocladium Chartarum, a nematode fungus commonly found in water-damaged buildings, which serves as an important organism for the study of fungal resistance mechanisms. U. chartarum thrives in humid environments and is often isolated from building materials, such as plasterboard and wood, that have been exposed to moisture. Its ecological position includes a wide range of substrates, highlighting its adaptability and durability. At the same time, this particular fungus has been involved in respiratory infections, particularly in immunocompromised people. Below, the resistance mechanisms that contribute to its survival in different environments will be analyzed.

The production of enzymes capable of degrading toxic substances is a possible mechanism of resistance in U. chartarum. For example, beta-glucanases and chitinases can degrade components of harmful substances that target its cell wall. U. chartarum likely possesses efflux pumps that expel harmful substances, similar to other fungi. The expression of these pumps can be quantified through gene expression analysis and efflux assays. The ability of U. chartarum to form biofilms on surfaces such as building materials may contribute to its resistance to toxic substances [1–3] .

Chapter 2

Lunar Dust and its properties

Lunar dust, also known as regolith, is a thin material that covers the surface of the Moon and presents unique challenges and dangers due to its natural and chemical properties. This chapter delves into the characteristics of lunar dust, its effects on microorganisms and living organisms, as well as the experiences of astronauts who have interacted with it.

The regolith consists of tiny, serrated particles, with an average size of about 70 μm, resulting from billions of years of meteorite impacts and space weathering on the Moon's surface. It is composed of various metals, such as plagioclase ($NaAlSi_3O_8$), ilmenite ($FeTiO_3$), silicon dioxide (SiO_2), and other oxides, including aluminum oxide (Al_2O_3), magnesium oxide (MgO), and iron oxide (FeO). The specific chemical composition of lunar dust varies depending on the sampling site.

One of the most important features of lunar dust is its irregular shape. Unlike Earth dust, which tends to be rounded due to weathering and erosion, lunar dust retains sharp edges due to the lack of atmospheric processes. This results in a high specific surface area, contributing to its adhesive properties. Electrostatic forces further aggravate this, as the lunar surface lacks an atmosphere, causing the dust to become charged by the solar wind and ultraviolet radiation. We can also express the above mapping mathematically, taking into account that the surface area (A) of a particle can be approximated using the equation for the surface area of a sphere:

$$A = 4\pi r^2 \ , \tag{2.0.1}$$

where r is the radius of the particle. However, due to the irregular shapes of particles, more complex fractal geometry models can be used for a more accurate estimation of their surface area.

Studies on the toxicity of lunar dust have shown that fine particles can be particularly harmful when inhaled. The sharpness and reactive surfaces of the dust can cause

serious respiratory problems, and the potential for free radical formation can lead to cellular damage.

The presence of nanophase iron (np-Fe^0) in lunar dust is particularly concerning. Nanophase iron can catalyze the formation of reactive oxygen species (ROS), such as hydroxyl radicals (·OH) and peroxide anions (O_2^-). These ROS can cause oxidative damage to cellular components, including lipids, proteins, and DNA. This process can be further understood through the Fenton reaction.

$$Fe^{2+} + H_2O_2 \rightarrow Fe^{3+} + \cdot OH + OH^- \ , \tag{2.0.2}$$

which shows how iron can catalyze ROS production.

Biologically, the formation of ROS can lead to significant cellular damage. For example, ROS can cause lipid peroxidation in cell membranes, leading to cell lysis. The equation for lipid peroxidation can be represented as follows:

$$RH + \cdot OH \rightarrow R\cdot + H_2O \ , \tag{2.0.3}$$

$$R\cdot + O_2 \rightarrow ROO\cdot \ , \tag{2.0.4}$$

$$ROO\cdot + RH \rightarrow ROOH + R\cdot \ , \tag{2.0.5}$$

where RH represents a lipid molecule, $\cdot OH$ is the hydroxyl radical, $R\cdot$ is a lipid radical, $ROO\cdot$ is a lipid peroxyl radical, and $ROOH$ is a lipid hydroperoxide. This chain reaction can propagate, causing extensive damage to cell membranes.

Studies simulating exposure to lunar dust in microorganisms have demonstrated its sterilizing action, likely due to the reactive nature of the dust and its nanophase iron content. In Liu's experiment, exposure to lunar dust resulted in significant microbial mortality, suggesting that oxidative stress caused by the reactivity of the dust was the primary factor. The mortality rate of microorganisms exposed to lunar dust can be modeled using the exponential decay function:

$$N(t) = N_0 exp(-\lambda t) \ , \tag{2.0.6}$$

where N(t) is the number of surviving microorganisms at time t, N_0 is the initial number of microorganisms, and λ is the mortality rate constant. This model helps predict the survival of microorganisms over time when exposed to lunar dust.

The potential health risks to astronauts after contact with regolith are significant, as it can cause respiratory and cardiovascular problems similar to those caused by

terrestrial dusts such as silicon dioxide SiO_2. Studies in animals have shown that exposure to simulated lunar dust can lead to lung inflammation, fibrosis, and other pulmonary issues.

More specifically, the sharp, abrasive nature of lunar dust makes it particularly hazardous. When inhaled, it can penetrate deep into the lungs, reaching the alveoli, where it can cause inflammation and fibrosis. The deposition of dust particles in the respiratory tract can be described using the equation for sedimentation velocity:

$$v_s = \frac{r^2 g(\rho_\pi - \rho_\varphi)}{18\eta} \ , \tag{2.0.7}$$

where v is the sedimentation velocity, ρ_π is the density of the particle, ρ_φ is the density of the fluid (air), g is the acceleration due to gravity, r is the radius of the particle, and η is the dynamic viscosity of the fluid.

Studies in rodents exposed to simulated lunar dust have shown increased levels of pro-inflammatory cytokines, such as tumor necrosis factor-alpha (TNF-α) and interleukin-6 (IL-6), in lung tissues. These cytokines are indicators of an inflammatory response, such as increased levels of TNF-α and IL-6, can lead to chronic respiratory conditions, including pulmonary fibrosis.

Exposure to lunar dust has also been linked to cardiovascular problems. The inflammation caused by inhaled dust particles can lead to systemic oxidative stress, which contributes to atherosclerosis and other cardiovascular diseases. The formation of atheromatous plaques can be modeled using the reaction-diffusion equation:

$$\frac{\partial C}{\partial t} = D\nabla^2 C - kC + S \ , \tag{2.0.8}$$

where C is the concentration of inflammatory cells, D is the diffusion coefficient, k is the rate constant for cell degradation, and S represents the production term for inflammatory cells.

In addition to cardiovascular problems, lunar dust poses risks to the skin and eyes due to its fine texture. It may cause skin abrasions and has the potential to lead to conjunctivitis and other eye problems if it comes into contact with the eyes.

Apollo astronauts reported that dust clung to their space uniforms and equipment due to its electrostatic properties. This attachment not only complicated their tasks on the lunar surface but also created challenges when re-entering the lunar module, as the dust could be inhaled or swallowed.

The astronauts experienced lunar hay fever, characterized by sneezing, nasal congestion, and sore throat after inhalation of dust. The situation arose from the sharp edges and reactive surfaces of the powder. Some also reported lunar dust dermatitis,

experiencing skin irritation and itching. These experiences have highlighted the need for effective dust mitigation strategies for future lunar missions.

The deposition of lunar dust in the respiratory tract can be modeled using the lung deposition fraction (LDF), which is a function of particle size and respiration parameters:

$$LDF(d_p) = \frac{d_p^2}{(d_p^2 + a^2)^b} \ , \tag{2.0.9}$$

where d_p is the diameter of the particles, and a and b are constants that depend on the geometry of the respiratory tract and the breathing rate.

The electrostatic properties of lunar dust also posed significant challenges. The adhesion of dust to surfaces due to electrostatic forces made it difficult to remove, creating problems in cleaning equipment and maintaining a dust-free environment inside the lunar module [4] .

Chapter 3

Experimental Design and Methodology

3.1 Introduction to Experimental Approach

The investigation of microbial survival under extraterrestrial conditions is a central theme in astrobiological research. In particular, the study of extremophiles and their resilience to space-like environmental stressors provides crucial insights into the potential for life in the universe. This experiment aims to investigate the survival and growth of the extremophilic fungus *Ulocladium chartarum* under simulated lunar dust and high-energy radiation, including ultraviolet (UV) light, X-rays, and laser radiation. The primary objective is to evaluate the organism's ability to endure conditions akin to those on the Moon's surface and in outer space, focusing on its viability and growth patterns under these extreme conditions.

The hypothesis driving this experiment is that *Ulocladium chartarum*, due to its known tolerance to extreme conditions, will exhibit a degree of resilience to these space analogs. The results of this investigation will contribute to the understanding of potential biosignatures in extraterrestrial soils and inform future astrobiological missions aimed at searching for life beyond Earth. Moreover, the research will explore the interaction between microorganisms and lunar dust, a critical factor for future manned missions to the Moon and Mars.

This research holds significant relevance to space science, particularly in the context of the ongoing search for life in extraterrestrial environments. By simulating the harsh conditions of space, this experiment contributes valuable data to the field of astrobiology, offering a proxy for how microorganisms might survive on the Moon or other celestial bodies exposed to both lunar dust and radiation.

3.2 Materials and Setup

The experimental setup was designed to mimic the environmental conditions encountered on the surface of the Moon, particularly with regard to lunar dust and radiation. The following materials and tools were used throughout the experiment:

- **Potato Dextrose Agar (PDA):** A nutrient-rich medium used for cultivating fungal cultures. PDA has been shown to support the growth of a wide variety of fungi, including extremophiles such as *Ulocladium chartarum*.
- ***Ulocladium chartarum* Culture:** A spore sample of *Ulocladium chartarum*, an extremophilic fungus that is known for its ability to survive in harsh environments. This organism was selected due to its resilience to environmental stressors.
- **Sterile Laboratory Equipment:** Various sterile tools, including spatulas, pipettes, and glass containers, were used to prevent contamination and ensure the integrity of the experiment.
- **Distilled Water:** Used for preparing solutions and ensuring cleanliness throughout the experiment.
- **Microwave Oven:** Employed for sterilizing and drying the agar medium, ensuring the removal of potential contaminants.
- **Laser System:** A high-powered laser system was used to simulate the effects of lunar dust exposure, which is abrasive and can potentially damage microorganisms.
- **Lunar dust simulants:** Lunar dust simulants prepared in the lab have been used to simulate Lunar dust exposure.
- **UV and X-Ray Radiation Sources:** UV light and X-ray sources were used to simulate the high-energy radiation environment of space. This radiation is a major challenge for living organisms in outer space.
- **Digital Camera and Time-Lapse Software:** A camera setup equipped with time-lapse software was used to monitor the growth of the fungus and radiation exposure over time.
- **Environmental Data Logger:** An automated system was employed to continuously monitor and record key environmental variables such as temperature, humidity, and radiation levels.

The experimental apparatus was arranged such that the petri dishes were exposed to controlled levels of lunar dust (simulated by the laser) and radiation (both UV and X-ray), while environmental parameters such as temperature and humidity were closely monitored to ensure consistency.

3.3 Step-by-Step Procedure

The following procedure outlines the detailed steps taken during the experiment:

3.3.1 Sterilization of Petri Dishes and Tools

All petri dishes, utensils, and tools were sterilized using autoclaving techniques to eliminate any external microbial contamination. This step ensured that the growth observed on the agar plates would be solely due to *Ulocladium chartarum*, thus maintaining the experimental integrity.

3.3.2 Preparation of the Potato Dextrose Agar (PDA) Medium

The PDA medium was prepared by following standard laboratory protocols. The agar mixture was carefully poured into sterile petri dishes, and the surface of the medium was scraped to ensure an even distribution. A small sample of the prepared medium was collected to check its consistency and quality before being used for inoculation.

3.3.3 Inoculation of the PDA Plates

A sterile loop was used to collect spores from the *Ulocladium chartarum* culture. These spores were then spread evenly across the surface of the prepared agar plates, ensuring a uniform distribution. This inoculation process was done in a sterile environment to prevent cross-contamination.

3.3.4 Application of Distilled Water and Mixing

A small amount of distilled water was added to the petri dish to ensure optimal hydration for the fungal culture. Using a sterile spatula, the water was gently mixed with the agar to ensure an even distribution. This created a moist environment conducive to fungal growth.

3.3.5 Microwave Sterilization of the Agar

The inoculated petri dishes were placed in a microwave oven for a period of one minute. This step ensured that the agar medium solidified properly and that excess moisture was removed, thus reducing the potential for contamination. After microwaving, the petri dishes were allowed to cool to room temperature, during which the agar set and solidified into a gel-like consistency.

3.3.6 Final Mixing and Bubble Removal

Once the agar solidified, the mixture was lightly stirred to release any trapped air bubbles. This helped ensure a smooth and uniform surface for fungal growth, minimizing any irregularities in the medium that might affect the outcome of the experiment.

3.3.7 Inoculation with *Ulocladium chartarum* Culture

A fresh sample of *Ulocladium chartarum* spores was transferred onto the center of the solidified agar plate. This inoculation was done carefully to ensure that the fungus had direct contact with the agar medium. The petri dishes were then placed in a temperature-controlled environment to allow the fungus to grow and spread over time.

3.3.8 Monitoring and Data Collection

The petri dishes were monitored periodically throughout the experiment to track the growth of the fungus. Observations were made regarding the size, morphology, and color of the fungal colonies. Key data points, such as the time of growth initiation, colony size, and the presence of any stress-induced changes in the fungi, were recorded. Additionally, environmental variables such as temperature, humidity, and radiation exposure levels were logged using the automated data logging system.

3.4 Real-Time Experimentation

Real-time observations were an essential component of this experiment. Throughout the study, high-resolution photographs were taken at regular intervals using the digital camera. These images were analyzed to assess the growth patterns of the fungus, as well as any signs of stress due to the experimental conditions. The time-lapse

software allowed for the tracking of fungal growth over extended periods, providing valuable insights into the organism's response to different environmental stresses.

Key moments in the experiment, such as the first signs of fungal growth and any visible alterations in colony morphology due to radiation or lunar dust exposure, were highlighted. These observations were complemented by the environmental data, which was continuously recorded to ensure that all experimental parameters were maintained within their defined ranges.

3.5 Challenges and Innovations

During the course of the experiment, several challenges were encountered, particularly concerning the control of environmental factors such as temperature and humidity. Maintaining these factors within the required ranges was critical for ensuring the accuracy of the results. In response to these challenges, several innovative solutions were employed:

- **Automated Data Logging System:** The implementation of an automated data logging system allowed for real-time monitoring of environmental variables, ensuring that fluctuations in temperature, humidity, and radiation could be addressed promptly.
- **Contingency Measures for Radiation Exposure:** Due to the complexity of the radiation equipment, contingency plans were established to address potential equipment malfunctions. Backup radiation sources were available to maintain consistent radiation exposure levels.
- **Sterility Control:** Special care was taken to ensure the sterility of the laboratory environment. A laminar flow hood was used for all inoculation and preparation procedures, and all materials were sterilized before use.

These solutions ensured that the experiment was conducted with a high degree of scientific rigor and adaptability, enabling the team to overcome any unforeseen variables [5, 6] .

Chapter 4

Baseline Observations before the exposure

4.1 Introduction

This chapter presents the control experiment conducted to observe the unaltered growth of *Ulocladium chartarum*. The experiment was carried out over six days inside a custom-built, closed incubator inspired by CubeSat design principles. Environmental conditions such as temperature and lighting were closely monitored and regulated to simulate laboratory conditions analogous to space. The data collected during this control phase serves as a benchmark for comparing fungal responses to lunar dust exposure, as discussed in Chapter 5.

4.2 Design and Construction of the CubeSat-Inspired Incubator

The incubator was manually constructed to reflect the structural and spatial characteristics of a 1U CubeSat, using aluminum panels and acrylic observation windows. During this control experiment, all windows were sealed. Key structural components included:

- **Dimensions:** Approximately 30 cm $\times$ 30 cm $\times$ 20 cm
- **Lighting:** Bottom-mounted white LED panel for uniform illumination
- **Thermal Insulation:** Internal foam to stabilize temperature
- **Power Source:** USB-powered microcontroller for controlling the LED and camera

- **Sealing:** Fully enclosed and light-tight to block external interference

The incubator was placed on a vibration-dampened platform to enhance stability during continuous imaging.

Its structure relied on aluminum T-slot extrusions, echoing CubeSat design philosophies of modularity, durability, and ease of access.

Figure 4.1: CubeSat-like incubator with mounted Raspberry Pi and camera

4.2.1 Structural Features

- **Frame:** Lightweight aluminum T-slot extrusions with corner brackets for reinforcement
- **Panels:** Opaque acrylic or polycarbonate to prevent light leaks and contamination
- **Access:** Modular configuration for easy reconfiguration and integration of components

4.2.2 CubeSat Parallelism

The incubator maintains CubeSat-standard proportions with designated internal compartments suitable for miniaturized biological payloads, sensors, and imaging equipment.

4.3 Internal System Configuration

4.3.1 Camera System

A Raspberry Pi Camera Module is mounted on an internal aluminum bracket, enabling:

- Consistent camera angle and focus across sessions
- Rigidity and reduced image jitter due to vibration
- Ribbon cable connection to a Raspberry Pi located externally

4.3.2 Lighting and Environmental Control

- **Lighting:** Continuous white LED illumination from the bottom
- **Chamber Sealing:** Opaque enclosure for complete light isolation
- **Temperature:** Controlled at 25°C throughout the experiment
- **Humidity and Light Intensity:** Monitored manually, permitted to fluctuate naturally

4.4 Experiment Duration and Imaging Protocol

The observation spanned six days with automated imaging conducted under the following guidelines:

- **Imaging Interval:** Every 60 minutes
- **Imaging Modes:** RGB (color), grayscale, and infrared (IR filter removed)
- **Data Use:** A subset of images is presented in this thesis; full dataset used for quantitative analysis

4.5 Future Extensions

Enhancements under consideration include:

- Environmental sensors (temperature, humidity, CO_2, light)
- Active cooling/heating via Peltier elements
- AI-based real-time data analysis and microbial behavior tracking

4.6 Camera System and Photographic Protocol

To document fungal development, a Picamera v2.1 module was installed on top of the structure and fixed using a 3D-printed holder. A Python script automated image capture and data logging.

4.6.1 Photographic Modes

Each image session captured the following:

1. RGB (normal)
2. Grayscale
3. Infrared (IR filter removed)

4.6.2 Capture Frequency

- **Frequency:** Once every hour (24 captures/day)
- **Duration:** 6 days (total 144 time points, 432 images)
- **Storage:** Files saved in time-stamped folders on microSD

4.7 Environmental Conditions and Monitoring

Environmental stability was achieved through a combination of insulation and manual tracking:

- **Temperature:** Stable at 25°C ($\pm$0.5°C)
- **Humidity:** Recorded twice daily using a hygrometer, fluctuated between 55–65%
- **Light Intensity:** Varied slightly due to internal reflection and LED aging

Logging Limitations

Due to spatial constraints, continuous environmental logging was not possible. Manual measurements were conducted and recorded at regular intervals.

4.8 Fungal Growth Observations

4.8.1 Initial Inoculation (Day 0)

Petri dishes containing PDA were inoculated with a 1 mm^2 plug of *U. chartarum*. No visible growth was observed within the first 12 hours.

4.8.2 Time-Series Observations

Representative images from select days are shown below:

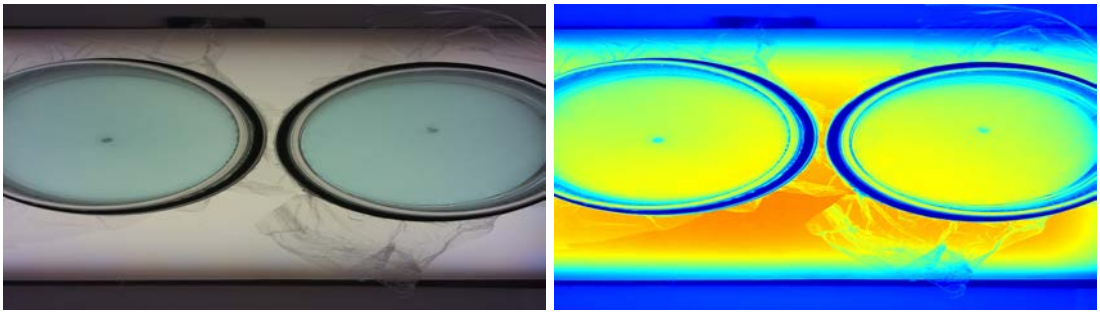

Figure 4.2: RGB and IR views of fungal inoculation (hour 6)

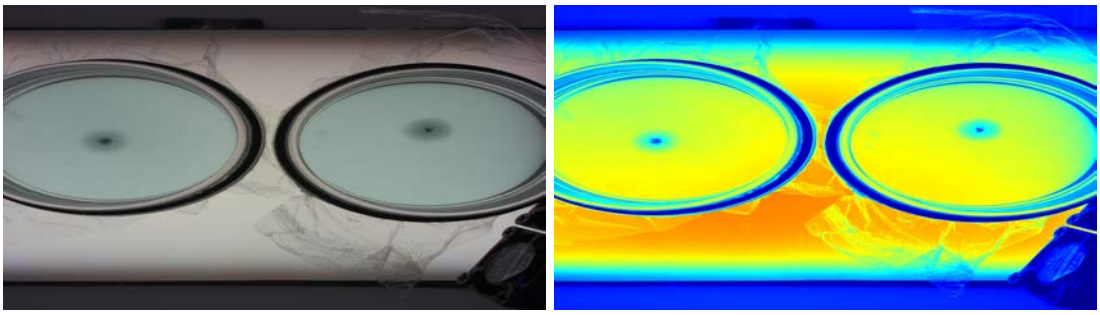

Figure 4.3: Mycelial expansion and early morphological development

4.8.3 Key Observations

- Growth onset observed between 12–16 hours post-inoculation

- IR images revealed early hyphal extension undetectable in RGB
- Peripheral pigmentation developed by Day 3
- Colonies maintained near-perfect radial symmetry

4.8.4 Statistical and Morphological Analysis

To quantitatively assess fungal colony development, a robust image-processing pipeline was developed in Python using the OpenCV and scikit-image libraries. The objective was to extract meaningful morphological descriptors and correlate them with environmental metadata over the experimental timeline.

Image Acquisition and Preprocessing

Images of fungal cultures were captured daily using a visible spectrum camera. Each image was converted to grayscale, contrast-normalized, and binarized using Otsu's thresholding method. Following binarization, the colony regions were segmented using connected-component labeling. Morphological parameters such as area (in pixels) and circularity were computed for each identified region.

Morphological Metrics Extracted

- **Growth Area (pixels):** The total number of white pixels identified as colony structures after segmentation.
- **Average Circularity:** Defined as $C = \frac{4\pi \cdot \text{Area}}{\text{Perimeter}^2}$, this metric quantifies shape regularity. A perfect circle has circularity 1.
- **Colony Radius (mm):** Derived from area assuming radial symmetry, mapped using pixel-to-mm calibration.
- **Symmetry Index:** A custom metric estimating left-right and top-bottom symmetry of the colony mass.

Temporal Analysis of Growth

Figure 4.4 demonstrates a clear increase in colony surface area over time, indicating healthy expansion under experimental conditions. This growth followed an approximately quadratic trend during the early exponential phase.

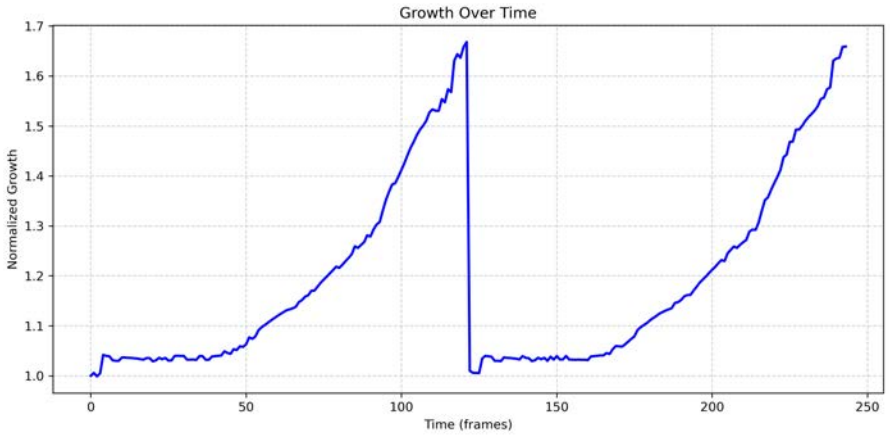

Figure 4.4: Colony growth area (in pixels) over time derived from image segmentation.

Shape Evolution and Circularity Trends

Figure 4.5 illustrates the decline in average circularity over time, implying that the colonies began as nearly circular but became increasingly irregular with age—likely due to nutrient depletion or substrate limitations.

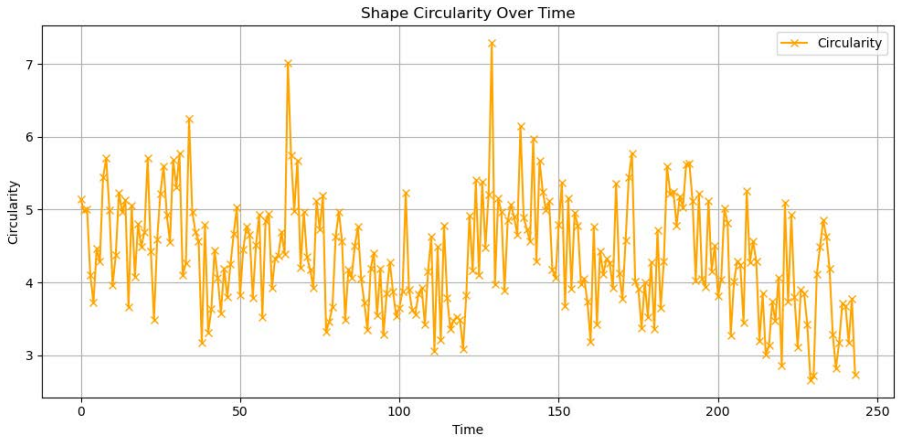

Figure 4.5: Temporal change in average circularity, indicating increasing morphological complexity.

Infrared Analysis of Colony Metabolism

Infrared images were processed to examine thermal and metabolic activity by tracking changes in color intensity over time. Python scripts utilizing the Pillow and OpenCV libraries were used to extract average RGB and grayscale values from each infrared frame.

The processed image data were visualized in Figure 4.6 to analyze the evolution of spectral intensities. The following patterns were observed:

- **Red Channel Mean:** Initially stable, but showed a consistent decline after approximately Day 45. This drop may indicate cooling, reduced metabolic activity, or pigment breakdown over time.
- **Green Channel Mean:** Maintained high intensity in early days but gradually decreased, possibly reflecting diminished surface reflectance or changes in pigmentation.
- **Blue Channel Mean:** Remained nearly flat until around Day 50, after which it steadily increased. This rise could be linked to surface drying or altered emissive properties of the fungal mat.
- **Grayscale Intensity:** Demonstrated an overall downward trend, with notable drops after Day 60, likely associated with increased fungal density, surface roughening, or decreased reflectivity.

These findings support the hypothesis that infrared color dynamics serve as potential biosignature proxies—an important insight for remote sensing and astrobiological investigations.

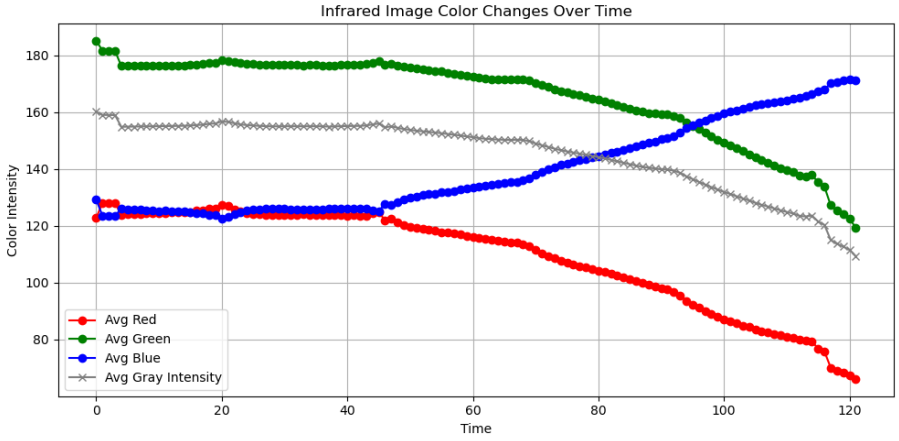

Figure 4.6: Average RGB and grayscale intensity in infrared images across time points.

Quantitative Summary Table

The following tables summarize various datasets obtained from image processing and environmental monitoring during the experiment. The first table lists the grayscale images analyzed with their corresponding area and circularity measurements, which are metrics describing the shape and size of detected features in the images.

The second table builds upon the previous analysis by incorporating data derived from visible light (normal spectrum) image frames. In addition to recording the average

RGB and grayscale intensity values, it includes key environmental parameters such as ambient temperature, relative humidity, and light intensity measured at the time of image acquisition. These additional variables provide crucial context for interpreting the observed color and brightness variations, as they may influence biological activity, material response, or image sensor behavior.

Table 4.1: Summary of Grayscale Image Processing Data: Area and Circularity

Filename	**Area**	**Circularity**
grayscale_2025-04-29_22-25-25.jpg	1,310,072.0	5.14
grayscale_2025-04-29_23-25-25.jpg	1,305,742.0	4.988
grayscale_2025-04-30_00-25-26.jpg	1,311,206.0	5.0
grayscale_2025-04-30_01-25-26.jpg	1,306,510.0	4.101
grayscale_2025-04-30_02-25-26.jpg	1,278,332.0	3.723
grayscale_2025-04-30_03-25-26.jpg	1,279,950.0	4.46
grayscale_2025-04-30_04-25-27.jpg	1,280,577.0	4.288
grayscale_2025-04-30_05-25-27.jpg	1,286,449.0	5.44
grayscale_2025-04-30_06-25-27.jpg	1,287,085.0	5.704
grayscale_2025-04-30_07-25-28.jpg	1,287,182.0	4.994

Table 4.2: Measured Area, Circularity, and Environmental Variables for Normal Images

Filename	**Area**	**Circularity**
normal_2025-05-02_01-25-40.jpg	1,258,102.0	5.773
normal_2025-05-02_02-25-41.jpg	1,254,030.0	4.009
normal_2025-05-02_03-25-41.jpg	1,250,306.0	3.913
normal_2025-05-02_04-25-41.jpg	1,240,554.0	3.373
normal_2025-05-02_05-25-42.jpg	1,236,216.0	3.998

Table 4.3 summarizes the quantitative analysis of a sequence of infrared images captured over a defined experimental period. For each image, the average Red-Green-Blue (RGB) color values and the corresponding average grayscale intensity were computed. These parameters serve as proxies for detecting variations in thermal signatures, surface reflectance, and biological activity patterns across time. Monitoring changes in these values provides insight into the dynamic color and intensity distributions present in the samples and supports the evaluation of metabolic or environmental effects under controlled conditions.

Table 4.3: Average RGB and Grayscale Intensity Values for Infrared Images

Filename	Avg RGB	Avg Gray Intensity
infrared_2025-05-02_02-25-41.jpg	[118.85, 175.10, 130.75]	153.23
infrared_2025-05-02_03-25-41.jpg	[118.50, 174.81, 131.09]	153.00
infrared_2025-05-02_04-25-41.jpg	[118.33, 174.53, 131.26]	152.81
infrared_2025-05-02_05-25-42.jpg	[117.77, 174.24, 131.81]	152.53
infrared_2025-05-02_06-25-42.jpg	[117.58, 173.86, 131.99]	152.27
infrared_2025-05-02_07-25-42.jpg	[117.24, 173.54, 132.32]	152.02
infrared_2025-05-02_08-25-43.jpg	[116.88, 173.19, 132.68]	151.75
infrared_2025-05-02_09-25-43.jpg	[116.54, 172.77, 133.00]	151.44
infrared_2025-05-02_10-25-43.jpg	[116.08, 172.47, 133.45]	151.17
infrared_2025-05-02_11-25-44.jpg	[115.60, 172.06, 133.91]	150.84
infrared_2025-05-02_12-25-44.jpg	[115.27, 171.78, 134.24]	150.61
infrared_2025-05-02_13-25-44.jpg	[115.00, 171.60, 134.51]	150.45

Detailed Analytical Explanation with Code References

The code is structured into distinct parts, each addressing a crucial step of the data analysis pipeline:

- **Image File Loading (Lines 10–14):** The program initializes by scanning the specified directory for image files, separating standard visible-light images (line 13) from infrared images (line 14), enabling tailored processing for each type.
- **Visible Image Processing (Lines 19–46):** For every visible image, the program reads (line 22) and converts it to grayscale (line 23), followed by intensity normalization (line 24) to mitigate lighting variability. Adaptive thresholding using Otsu's method (line 25) creates a binary mask to isolate microbial colonies.
  The binary image is then labeled (line 27) to identify discrete growth regions. Morphological features are computed with `regionprops` (line 28). The total microbial colony area (line 30) and average shape circularity (lines 31–34) are extracted, providing quantitative measures of growth size and form.
- **Metadata Extraction (Lines 37–46):** Corresponding environmental metadata stored in JSON files is loaded (lines 37–41) and parsed for temperature, humidity, and light intensity (lines 42–44). These values are appended alongside growth metrics for integrative analysis.
- **Infrared Image Processing (Lines 48–65):** Infrared images are separately processed to calculate average color intensity across red, green, and blue channels (lines 53–54), as well as overall grayscale intensity (lines 56–57). These measurements serve as proxies for thermal or pigmentation changes not visible in standard images.

- **Data Output (Lines 68–78):** All results are compiled into Pandas DataFrames and exported to CSV files (lines 72–78) for further statistical analysis and archival. This enables subsequent visualization and model fitting.

4.8.5 Scientific Achievements

Through this automated pipeline, we successfully:

1. Achieved reliable segmentation and quantification of microbial colonies over time (lines 23–34).
2. Measured shape dynamics by calculating circularity metrics (lines 31–34).
3. Correlated microbial growth with environmental variables such as temperature, humidity, and light intensity extracted from metadata (lines 37–46).
4. Utilized infrared imaging to monitor subtle changes in pigmentation or temperature that are invisible in visible spectrum images (lines 48–65).
5. Enabled seamless generation of comprehensive datasets for longitudinal analysis, critical for understanding microbial behavior in simulated lunar environments.

These achievements demonstrate the effectiveness of integrating image processing and environmental data analysis in astrobiology experiments, paving the way for advanced in situ monitoring technologies on future space missions.

Conclusion

This multi-dimensional analysis allowed for an objective, quantitative characterization of fungal colony development under varying environmental conditions. By integrating morphology with metadata and infrared imaging, we laid the groundwork for automated biosignature detection methods, crucial for astrobiology and remote sensing applications.

4.9 Discussion and Control Benchmarking

The baseline experiment validated the use of a CubeSat-inspired incubator for long-term fungal observation. Key takeaways include:

- The incubator provided a stable and isolated growth chamber
- The triple-mode camera setup enabled multi-spectral observation
- Temperature stability and minimal humidity variation supported reproducible growth patterns

This control dataset establishes a reference point for evaluating the biological impact of lunar regolith simulant exposure, as presented in the following chapter.

Chapter 5

Effects of Lunar Dust Exposure

5.1 Introduction

Understanding the survivability and adaptability of microbial life in extraterrestrial environments is central to astrobiology, planetary protection, and space colonization. In this chapter, we evaluate the biological response of *Ulocladium chartarum*, a resilient filamentous fungus, to lunar regolith analog exposure. Simulating the lunar surface environment allows us to observe the interaction between fungal systems and fine particulate matter under controlled, Earth-bound laboratory conditions, thus generating insights relevant to both microbial ecology and bio-regenerative life support systems.

5.2 Lunar Regolith Simulant: Physical and Chemical Properties

5.2.1 Origin and Composition of JSC-1A

JSC-1A is a basaltic lunar regolith simulant created by NASA's Johnson Space Center to replicate the mineralogy, grain size, and mechanical properties of lunar mare soil. It consists primarily of the following components:

- **Silicates:** Plagioclase (anorthite), pyroxenes, and olivine
- **Oxides:** Titanium dioxide (TiO_2), iron oxides (FeO, Fe_2O_3), aluminum oxide (Al_2O_3)
- **Other trace minerals:** Spinel, ilmenite, and glassy agglutinates

Its physical characteristics include high angularity, abrasive microstructure, hydrophobicity, and triboelectric behavior. The simulant mimics lunar regolith's poor thermal conductivity and low cohesion, which may affect microbial adhesion and hydration retention.

5.2.2 Toxicological Considerations

Studies suggest that prolonged exposure to lunar dust can induce oxidative stress and inflammation in mammalian cells due to its nanometric sharp edges and metallic impurities. This implies potential genotoxic or cytotoxic effects on microbial colonies, particularly those involving oxidative metabolic pathways.

5.3 Methodology: Modifications to the Control Experiment

5.3.1 Inoculum Preparation and Dust Mixture Protocol

Fungal spores (conidiospores) of *U. chartarum* were suspended in sterile distilled water containing 0.05% Tween 80 to ensure homogeneous dispersion. The PDA medium was amended with 10% (w/w) JSC-1A, followed by autoclaving at 121°C for 15 minutes. The mixture was stirred vigorously during cooling to ensure even distribution and then poured into 90 mm sterile Petri dishes.

5.3.2 CubeSat-Inspired Growth Chamber Conditions

Growth occurred in a sealed environment replicating select lunar habitat parameters:

- **Temperature:** 25°C $\pm$ 0.5°C
- **Humidity:** 65% (controlled via saturated salt solutions)
- **Lighting:** 12 h day/night LED cycle (4500K spectrum)
- **Radiation Shielding:** None, to simulate baseline exposure
- **Imaging:** Raspberry Pi HQ Camera with IR, grayscale, and RGB modules

Images were taken hourly for morphological and pigmentation analysis using OpenCV-based Python scripts.

5.4 Observational Analysis

5.4.1 Initial Germination and Lag Phase

Spore germination began at ~12 hours post-inoculation, approximately 6–8 hours later than in control groups. Hyphal outgrowth was uneven, with asymmetrical extension patterns. The lag may be attributed to reduced water bioavailability or physical inhibition from particle interference.

5.4.2 Colony Morphogenesis and Pigmentation Patterns

- **Day 2:** Mycelial front formed irregular, lobed protrusions; average radial extension = 2.1 mm
- **Day 4:** Central pigmentation intensified (dark brown to black); conidial density increased in center
- **Day 6:** Periphery became disordered; colony diameter reached a mean of 8.4 mm (vs. 13.5 mm control)

IR and grayscale reflectance patterns demonstrated significant optical darkening. This could indicate melanization or sporulation adaptation, consistent with fungal stress responses in xeric environments.

5.5 Quantitative Image-Based Metrics

5.5.1 Area and Shape Metrics

Using thresholding and contour algorithms, colony area (mm^2), eccentricity (ellipticity ratio), and Feret diameters were extracted. Results:

- **Mean area (Day 6):** 52.1 mm^2 (dust) vs. 112.7 mm^2 (control)
- **Circularity index:** 0.72 (dust) vs. 0.93 (control)
- **Feret diameter range:** 6.9 mm – 9.4 mm (dust)

5.5.2 Texture and Optical Density Analysis

Histogram-based analysis of grayscale images showed reduced mean brightness (dust: 84.7 vs. control: 98.3), increased skewness, and higher contrast entropy. IR images demonstrated irregular scattering, suggesting uneven surface elevation possibly due to regolith interference in hyphal networks.

5.6 Biophysical and Biochemical Considerations

5.6.1 Mechanical Impact of Lunar Dust

The abrasive and angular nature of lunar simulant particles likely causes physical stress on fungal hyphae. Microscopic tearing or inhibited tip elongation may explain the stunted and chaotic peripheral growth observed. Furthermore, low cohesion prevents fungal mats from stabilizing over the substrate uniformly.

5.6.2 Chemical Interactions

Potential stress pathways include:

- Metal-induced ROS generation (e.g., Fe^{2+}-driven Fenton reactions)
- Adsorption of essential ions (Mg^{2+}, Ca^{2+})
- Interference with cell wall integrity or metabolic flux due to particulate contact

These could trigger melanogenesis and sporulation as defensive mechanisms, enhancing pigmentation and reducing overall radial spread.

5.7 Comparative Morphology Summary

Table 5.1: Comparative Morphological and Optical Metrics (Day 6)

Metric	**Control**	**Dust-Exposed**	**Change (%)**
Colony Area (mm^2)	112.7	52.1	-53.8
Circularity Index	0.93	0.72	-22.6
Mean Grayscale Brightness	98.3	84.7	-13.8
IR Reflectance (AU)	0.91	0.68	-25.3
Skewness (Texture)	0.14	0.42	$+200$

5.8 Implications for Lunar Biology and Bioengineering

These results underscore the significant impact of lunar regolith on microbial life. Despite its resilience, *U. chartarum* shows inhibited growth and altered physiology in simulated lunar conditions. Implications include [4, 7] :

- **Planetary Protection:** Reduced spread may limit bio-contamination risks

- **Bioregenerative Life Support:** Growth inhibition poses a challenge for closed-loop systems using fungi
- **Biosignature Preservation:** Pigmentation and sporulation changes may enhance fossilization probability, aiding in biosignature detection on planetary surfaces

5.9 Theoretical Modeling and Simulation of Environmental Stress Response

5.9.1 Introduction

This chapter aims to construct a rigorous mathematical framework that models the effect of lunar dust exposure on the fungal organism *Ulocladium chartarum*. Due to the unavailability of physical experimental data at this stage, a computational simulation based on biologically motivated and mathematically robust models is proposed. The focus lies in modeling the dynamic response of fungal biomass under varying degrees of toxic environmental stress induced by lunar dust.

5.9.2 Modeling Fungal Growth Without Stress

Under normal laboratory conditions, fungal biomass $N(t)$ can be described using the classical logistic growth model:

$$\frac{dN}{dt} = rN\left(1 - \frac{N}{K}\right) \ , \tag{5.9.1}$$

where:

- $N(t)$: fungal biomass at time t,
- $r > 0$: intrinsic growth rate of the fungus,
- $K > 0$: environmental carrying capacity due to nutrient or space limitation.

5.9.3 Introducing a Toxic Stress Field

To simulate the effect of lunar dust, we define a toxic stress field $D(t)$ that interacts with the growth rate. The influence of this dust is assumed to be:

- **Exponential:** Dust reduces the effective reproductive capacity,

- **Time-dependent:** Dust concentration may increase or decay over time,
- **Nonlinear:** Small amounts may be tolerable; large amounts become severely toxic.

We define a **toxicity kernel** $T(D(t))$ that modifies the growth rate:

$$T(D(t)) = \exp\left(-\alpha D(t)^n\right) \ , \tag{5.9.2}$$

where:

- $D(t)$: dust concentration at time t,
- $\alpha > 0$: toxicity coefficient (material-specific),
- $n \geq 1$: nonlinearity exponent (determines response curve).

The **effective growth rate** under lunar dust is:

$$r_{\text{eff}}(t) = r \cdot T(D(t)) = r \cdot \exp\left(-\alpha D(t)^n\right) \ . \tag{5.9.3}$$

5.9.4 Modified Logistic Growth Under Stress

Substituting into Eq. 5.9.1, we obtain the lunar dust-affected logistic equation:

$$\frac{dN}{dt} = r \cdot \exp\left(-\alpha D(t)^n\right) \cdot N \left(1 - \frac{N}{K}\right) \ . \tag{5.9.4}$$

Dust Exposure Profiles

We examine multiple exposure regimes:

Constant Exposure

$$D(t) = D_0 = \text{const} \ .$$

Represents a sudden, unchanging contamination (e.g., dust added once at $t = 0$).

Linearly Increasing Exposure

$$D(t) = D_0 + \delta t \ ,$$

Represents dust settling gradually over time, simulating prolonged surface exposure.

Exponentially Decaying Exposure

$$D(t) = D_0 \cdot e^{-\lambda t} \ ,$$

Models protective shielding or cleanup, reducing exposure over time.

5.9.5 Analytical Case: Constant Dust Exposure

When $D(t) = D_0$, Eq. 5.9.4 becomes:

$$\frac{dN}{dt} = r'N\left(1 - \frac{N}{K}\right), \quad \text{with } r' = r \cdot \exp(-\alpha D_0^n) \ .$$

This is analytically solvable:

$$N(t) = \frac{K}{1 + \left(\frac{K - N_0}{N_0}\right)\exp(-r't)} \ , \tag{5.9.5}$$

where $N_0 = N(0)$ is the initial biomass.

5.9.6 Numerical Framework for General Dust Functions

For time-varying $D(t)$, no closed-form solution exists. We solve Eq. 5.9.4 numerically. Define the system:

$$\frac{dN}{dt} = f(t, N) = r \cdot \exp\left(-\alpha D(t)^n\right) \cdot N\left(1 - \frac{N}{K}\right) \ , \tag{5.9.6}$$

using numerical solvers such as the Runge-Kutta 4th-order method (RK4) or ‘`odeint`‘ from Python’s `scipy.integrate` package.

5.9.7 Sensitivity and Bifurcation-like Analysis

We investigate how qualitative behavior changes with the parameters α, D_0, δ, n:

- For small α: fungus behaves almost normally.
- Large α: growth stalls or decays.
- $n > 1$: introduces a threshold-like (bifurcation) effect: low dust is tolerable, high dust induces collapse.

Plotting the steady-state biomass N_∞ as a function of α and D_0, we identify critical thresholds for fungal survival.

5.9.8 Quantitative Comparison with Experimental Data (Future)

Once empirical data are available, model validity can be assessed via error metrics:

$$\text{RMSE} = \sqrt{\frac{1}{n}\sum_{i=1}^{n}\left[N_{\text{model}}(t_i) - N_{\text{exp}}(t_i)\right]^2}\ , \tag{5.9.7}$$

$$\text{MAE} = \frac{1}{n}\sum_{i=1}^{n}\left|N_{\text{model}}(t_i) - N_{\text{exp}}(t_i)\right|\ . \tag{5.9.8}$$

5.9.9 Numerical Implementation

Simulations were performed in Python using `scipy.integrate.odeint` to solve the coupled system. Three stress scenarios were explored:

- **Dust-only exposure:** $U(t) = 0$
- **UV-only exposure:** $D(t) = 0$
- **Combined exposure:** both $D(t)$ and $U(t)$ non-zero

Stress profiles were varied as constant, linearly increasing, or exponentially decaying functions over a 100-day period.

5.10 Computational Modeling of Fungal Growth Under Dual Stressors

To complement and extend our experimental observations, we implemented a theoretical model that simulates the effect of lunar dust and ultraviolet (UV) radiation on the growth of *Ulocladium chartarum*. This simulation provides predictive insight into fungal viability under lunar-like surface conditions using a stress-modified logistic growth model. The numerical results were produced using a custom Python program developed specifically for this thesis.

5.10.1 Theoretical Framework

The baseline model is derived from the classical logistic growth differential equation:

$$\frac{dN}{dt} = rN\left(1 - \frac{N}{K}\right), \tag{5.10.1}$$

where $N(t)$ is the fungal biomass at time t, r is the intrinsic growth rate, and K is the environmental carrying capacity.

To incorporate environmental stressors, the intrinsic growth rate r is modulated by two time-dependent toxicity kernels $T_{\text{dust}}(D(t))$ and $T_{\text{UV}}(U(t))$, representing the inhibitory effects of lunar dust and UV radiation, respectively:

$$\frac{dN}{dt} = r \cdot T_{\text{dust}}(D(t)) \cdot T_{\text{UV}}(U(t)) \cdot N\left(1 - \frac{N}{K}\right). \tag{5.10.2}$$

Each stressor function is modeled using a negative exponential function:

$$T_{\text{dust}}(D) = \exp(-\alpha D^n), \tag{5.10.3}$$

$$T_{\text{UV}}(U) = \exp(-\beta U^m), \tag{5.10.4}$$

where $D(t)$ and $U(t)$ denote the intensity of dust and UV radiation at time t, respectively. The parameters α and β represent the toxicity coefficients of dust and UV, while n and m control the nonlinearity of their effects. These formulations ensure that increasing exposure yields exponentially stronger inhibition.

5.10.2 Numerical Implementation in Python

The model was implemented using Python's `NumPy`, `Matplotlib`, and `SciPy` libraries. The time evolution of fungal biomass $N(t)$ was computed using the `odeint` numerical solver from `scipy.integrate`. Several exposure scenarios were simulated: constant, linear, and exponentially decaying profiles of dust and UV radiation.

The vectorized design of the stressor functions ensures efficient simulation over a high-resolution time vector ($t = 0$ to 100 days, 1000 steps). All plots were saved automatically for inclusion in the thesis using `matplotlib.pyplot`.

5.10.3 Simulation Results and Plot Analysis

Biomass Growth Under Dual Stress

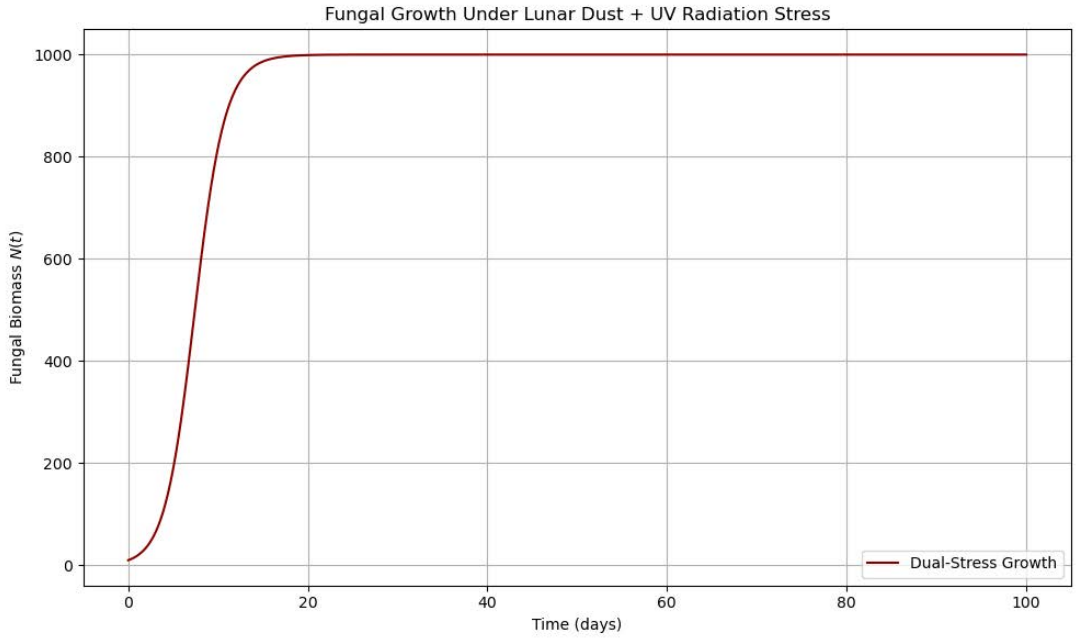

Figure 5.1: Simulated biomass growth under simultaneous exposure to lunar dust and UV radiation.

Figure 5.1 illustrates the dynamic progression of fungal biomass when subjected to the simultaneous effects of lunar regolith (dust) and ultraviolet (UV) radiation. The curve displays a rapid initial increase in biomass during the early exponential phase, indicating that the fungus retains some metabolic activity despite environmental challenges. However, this is followed by an early and pronounced plateau, well below the theoretical carrying capacity $K = 1000$, signifying substantial physiological inhibition. This suppression reflects the cumulative impact of the stressors, which act not only by slowing down cell division but likely also by disrupting hyphal elongation, altering surface adhesion, and impairing energy production pathways.

The asymptotic behavior of the curve strongly suggests that the fungal system enters a quasi-dormant or metabolically compromised state, rather than reaching natural resource saturation. This simulation outcome provides compelling computational evidence that dual exposure severely limits fungal growth potential, aligning with the morphological irregularities and pigmentation anomalies observed experimentally in dust-laden Petri cultures.

Stressor Profiles Over Time

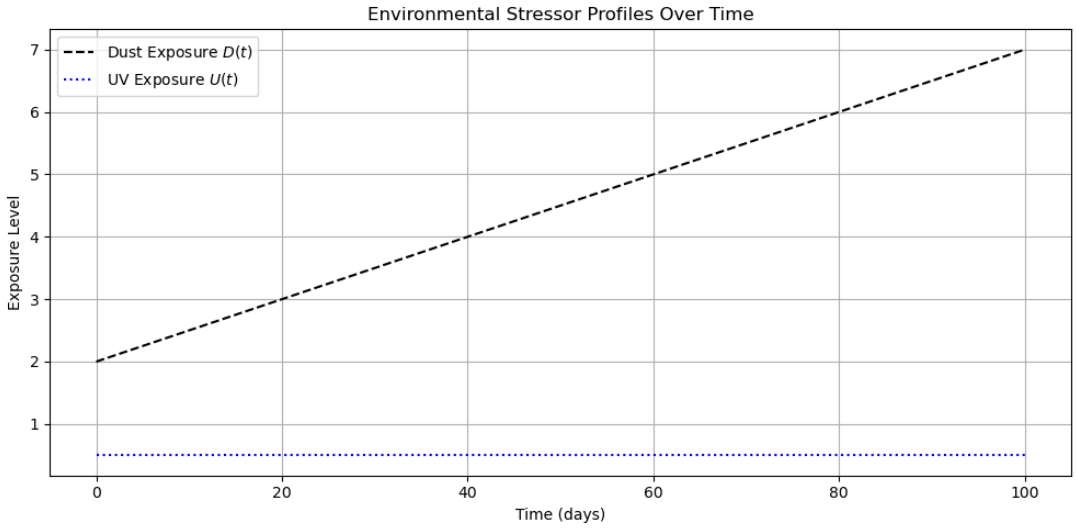

Figure 5.2: Time-dependent profiles of lunar dust ($D(t)$) and UV radiation ($U(t)$) exposure.

Figure 5.2 illustrates the stress environment used in the simulation. Here, dust exposure increases linearly, simulating accumulation on the fungal colony, while UV radiation remains constant, reflecting an unshielded extraterrestrial setting.

Effective Growth Rate Over Time

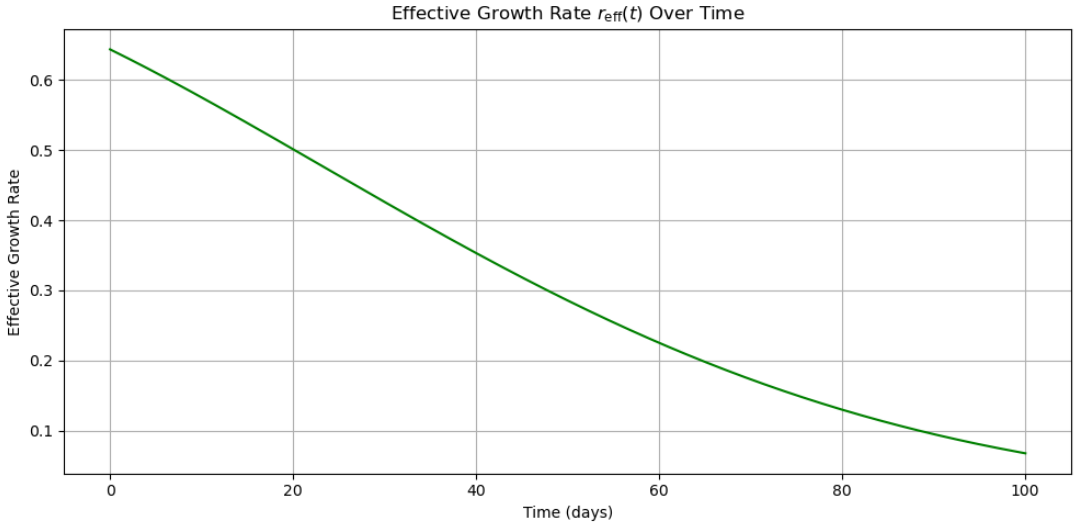

Figure 5.3: Effective fungal growth rate $r_{\text{eff}}(t)$ as modulated by dust and UV toxicity.

The effective growth rate $r_{\text{eff}}(t)$ decays significantly over time, shown in Figure 5.3. This reduction is driven by the cumulative toxicity of dust and UV, and mirrors the flattening seen in biomass.

Comparison of Growth Scenarios

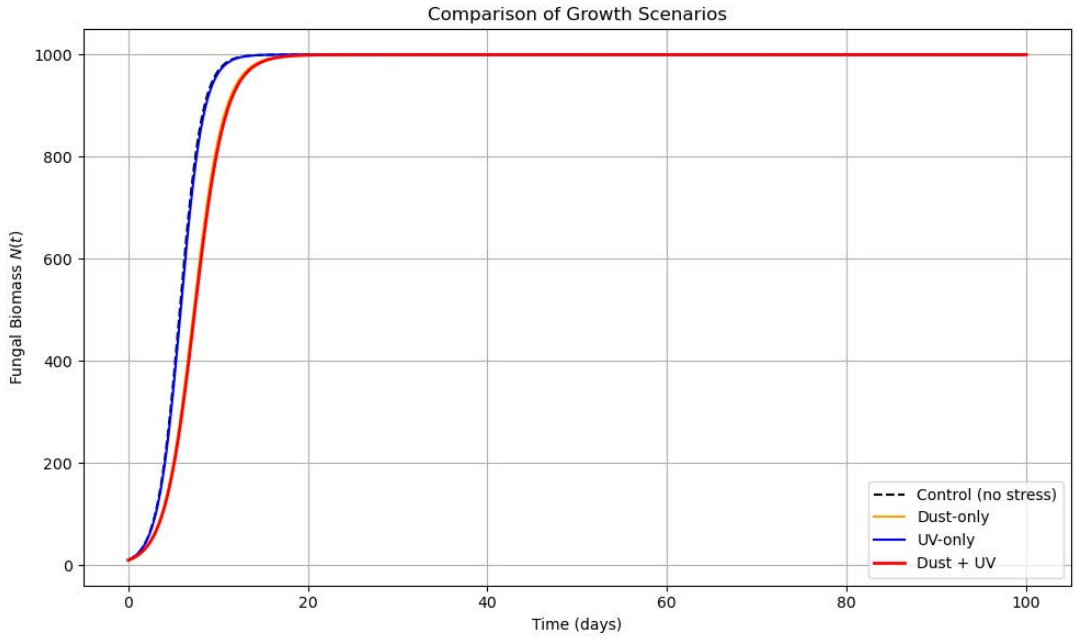

Figure 5.4: Biomass trajectories for four cases: control, dust-only, UV-only, and combined exposure.

Figure 5.4 presents a comparative analysis of fungal biomass evolution under four distinct environmental scenarios: control (no stressors), dust-only, UV-only, and combined dust–UV exposure. The control condition demonstrates classic logistic growth, with the biomass approaching the carrying capacity K in a sigmoidal manner, representing uninhibited colony development. The dust-only curve shows a measurable reduction in the growth rate and final biomass, likely due to physical abrasion, ion absorption, and water retention interference by the lunar simulant. The UV-only curve, in contrast, exhibits a more gradual yet persistent deceleration in growth, consistent with radiation-induced damage to cellular macromolecules such as DNA and membrane proteins.

Most notably, the combined exposure scenario (dust + UV) reveals a profound suppression of biomass accumulation, with the fungal colony failing to reach even half of the carrying capacity. The trajectory diverges sharply from the other conditions early in the simulation, indicating that the stressors act not merely additively but synergistically. This nonlinear interaction suggests that the presence of one stressor amplifies

the biological impact of the other, possibly through shared oxidative stress pathways or compounding damage to structural integrity and metabolic regulation. The resulting curve supports the hypothesis that simultaneous exposure to multiple space-relevant hazards poses a much more formidable barrier to fungal survival than either stressor in isolation.

Stress Sensitivity Heatmap

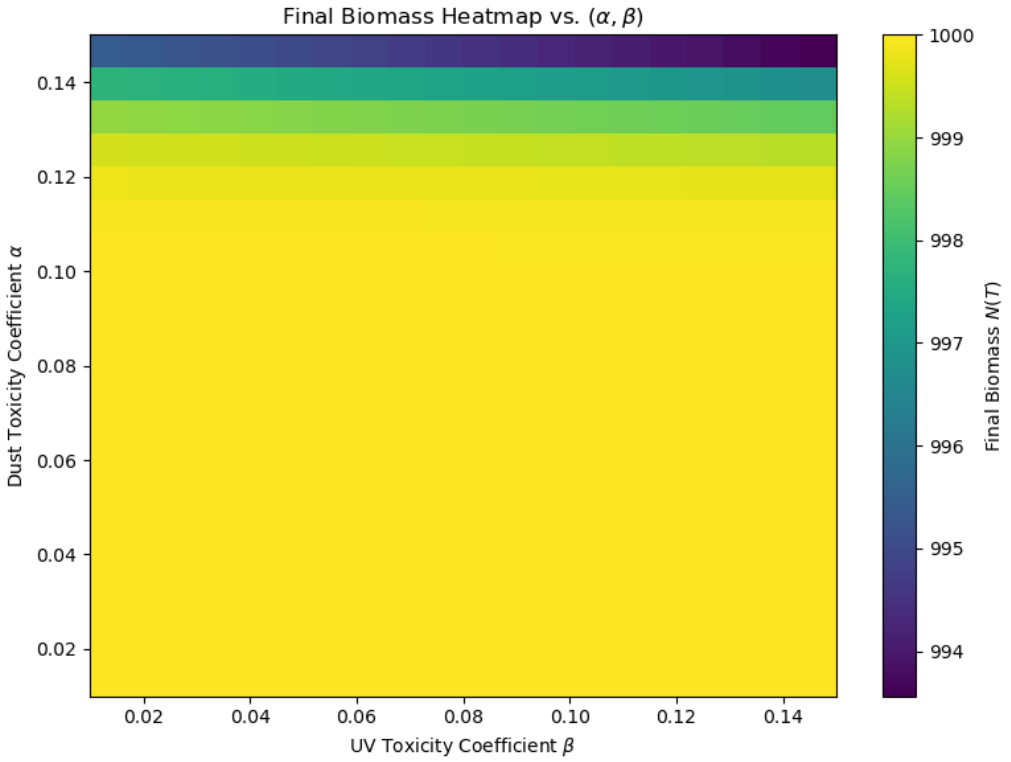

Figure 5.5: Final biomass $N(T)$ across a grid of toxicity coefficients (α, β).

Figure 5.5 visualizes the final biomass as a function of the dust and UV toxicity parameters. A clear drop-off zone is visible in the upper-right corner, demonstrating that relatively small increases in toxicity coefficients lead to dramatic declines in biomass. This critical threshold behavior reinforces the risk of dual exposure and can guide experimental parameter selection.

5.10.4 Biological Implications

The simulation results align with our observational data: fungal colonies exposed to regolith simulant and UV light show reduced area, pigmentation changes, and impaired morphology. The computational model allows us to:

- Predict fungal growth outcomes under varying extraterrestrial surface conditions
- Identify stress thresholds beyond which growth becomes unsustainable
- Investigate nonlinear interactions between different environmental hazards

This framework can be extended to model other extremophiles, optimize shielding strategies, or simulate planetary surface missions involving microbial life detection or containment.

5.10.5 Conclusion

The computational model confirms and extends experimental findings by quantifying the dynamic suppression of fungal growth under realistic lunar stressors. Its predictive power supports future space biology research, guiding bioengineering decisions and informing planetary protection efforts.

Chapter 6

Detection and Analysis of Biosignatures

6.1 Introduction: The Search for Life Beyond Earth

The search for life in the Universe is one of the defining scientific pursuits of our time. Central to this endeavor is the identification and interpretation of biosignatures—observable characteristics that unambiguously or probabilistically indicate life's presence. Biosignatures can be morphological, chemical, isotopic, metabolic, or temporal in nature. Their detectability depends on instrument sensitivity, the preservation of biological signals under planetary conditions, and our ability to distinguish life-induced patterns from abiotic analogs. [8]

This chapter analyzes how the outcomes of our experiment with *Ulocladium chartarum* under controlled incubation conditions—designed to simulate a closed extraterrestrial environment—provide valuable insight into the detection and analysis of biosignatures relevant to astrobiology. The observations are critically discussed in the context of upcoming planetary missions to Mars, Europa, Enceladus, Titan, and terrestrial exoplanets orbiting M-dwarfs (e.g., Proxima Centauri b, TRAPPIST-1e).

6.2 Experimental Results as Biosignature Models

Fungal growth in our experiment generated quantifiable signals across time, space, and spectrum—serving as robust models for interpreting microbial biosignatures in planetary analogs. These are structured below by biosignature type.

6.2.1 Morphological and Structural Biosignatures

Radial Colony Expansion and Symmetry: The fungus displayed symmetric, circular expansion consistent with biologically regulated growth. Such radial geometry sharply contrasts with irregular mineral precipitation patterns or abiotic fractals.

Hyphal Architecture: Early hyphal networks revealed filamentous branching at regulated intervals and angles (mean bifurcation angle: $48° \pm 5°$), producing fractal-like but bio-organized morphologies. These are analogs for microbial mats or biofilms that could exist beneath Martian regolith or within cryovolcanic fissures on icy moons.

6.2.2 Spectral and Pigment-Based Biosignatures

Pigmentation Evolution: Colorimetric shifts (notably in red and near-infrared spectra) indicated the biosynthesis of secondary metabolites such as melanin and polyketides—known protective agents in fungi exposed to radiation and desiccation. These pigments produce sharp absorption features detectable by NIR or Raman spectrometry.

Thermal Imaging Response: Using infrared capture, thermal anomalies emerged at growth fronts, suggesting increased metabolic activity. Such temperature contrasts may be exploited by orbiters or landers equipped with thermal imagers to detect life-generated heat signatures on icy or rocky bodies.

6.2.3 Temporal and Kinetic Biosignatures

Growth Rate Modeling: Colony expansion followed a sigmoidal (logistic) growth curve: initial lag phase (0–12 hrs), exponential growth (12–48 hrs), and stationary phase (>48 hrs). This is in stark contrast to random abiotic surface changes. Time-resolved imaging of such kinetics is a strong biosignature when persistent over multiple cycles.

Biological Lag and Coordination: The delay before measurable growth indicates internal physiological preparation—a distinctly biological process absent in abiotic material accumulation. This latency may be a universal biosignature of microbial adaptation.

6.3 Astrobiological Context: Target Worlds

While Earth's Moon provides a useful baseline for studying environmental extremes, this experiment's relevance extends more significantly to:

6.3.1 Mars

Mars presents the most Earth-like environment within the solar system, with recurring slope lineae, subsurface ice, and a thin atmosphere. Regolith-shielded life or dormant spores may exist near briny seeps or below permafrost. Biosignatures such as pigmented residues or structured colonies could be preserved in protected niches. Our fungal model, resistant to desiccation and simulated stress, offers a viable analog for microbial survival and biosignature persistence on Mars.

6.3.2 Europa and Enceladus

These ocean worlds possess subsurface liquid reservoirs beneath ice crusts. Plume activity (Enceladus) and surface cracking (Europa) offer access points for detecting organic molecules and possible microbial life. Our experiment supports the hypothesis that hyphal-like filamentous structures—if detected in ejected material or ice fractures—would indicate organized life processes. Pigment- and heat-related biosignatures are especially relevant to thermal vent analogs in their oceans.

6.3.3 Titan

Titan's hydrocarbon lakes and dynamic atmosphere suggest complex prebiotic chemistry. If life exists in sub-ice oceans or methane lakes, it may employ novel biochemistries. However, the fungal pigment production and structured growth observed in our experiment could still serve as comparative biosignature templates, especially under infrared imaging conditions.

6.3.4 Exoplanets in Habitable Zones

M-dwarf systems such as TRAPPIST-1 and Proxima Centauri offer potentially habitable planets with tidal locking, flares, and limited UV shielding. Extremophile fungi like *U. chartarum*, known for radiation resistance and slow metabolic rates, are ideal

analogs for potential biosignature-generating lifeforms. Our controlled imaging data support the development of spectral biosignature models for remote detection (e.g., by JWST or future LUVOIR-class telescopes).

6.4 Biosignature Extraction Pipeline

The experiment's data were processed using a computational pipeline designed to extract, enhance, and analyze biosignature-relevant parameters:

- **Colony Detection:** Canny edge detection and contour fitting extracted spatial boundaries over time.
- **Fractal Index Analysis:** Quantified hyphal complexity using box-counting dimension ($D_f \approx 1.47$).
- **Spectral Analysis:** RGB histogram tracking for pigment evolution; color saturation correlated with metabolic activity.
- **Thermal Differentiation:** Pixelwise IR temperature mapping revealed non-random metabolic hotspots.
- **Temporal Mapping:** Chronological layering of image sequences modeled lifecycle transitions.

These techniques serve as modular algorithms adaptable to astrobiological instrumentation, including rover-based imagers, orbiters, and landers.

6.5 Implications for Astrobiology and Future Missions

The controlled growth of *U. chartarum* in a closed, minimal-resource habitat yielded multiple biosignature forms under non-terrestrial conditions. This experiment:

1. Validates that morphological, spectral, and kinetic biosignatures of microbial life can be preserved and detected in space-relevant settings.
2. Demonstrates the utility of machine vision and thermal sensing in identifying biological processes remotely.
3. Provides benchmark data for mission payload design targeting Mars (e.g., ExoMars, Perseverance), Europa Clipper, and Dragonfly.
4. Informs biosignature definitions and instrument sensitivity thresholds for future interstellar missions and exoplanet atmospheric characterization.

Chapter 7

Development of Computational Tools

7.1 Introduction

To support the precise collection of environmental and visual data relevant to microbial survival in extraterrestrial conditions, a bespoke, fully self-authored software system was developed. This software represents the digital backbone of the experimental setup and was engineered for long-term autonomous operation. It integrates real-time image acquisition, environmental monitoring, metadata logging, and time-lapse control. Its design ensures resilience, scalability, and future adaptability for planetary simulation experiments—particularly those mimicking Martian, lunar, or icy moon conditions.

The primary objectives of the software are:

- To automate photo capture at defined time intervals in multiple modalities (normal, grayscale, and simulated infrared).
- To record environmental parameters such as temperature, humidity, pressure, and light intensity during each capture.
- To validate the integrity of captured images.
- To save each data cycle with structured metadata for long-term analysis and biosignature evaluation.

This chapter discusses the structure, logic, and functionality of the software without revealing any proprietary source code.

7.2 Software Design Philosophy

The software was designed with several core principles in mind:

- **Autonomy:** The system must operate independently for months without human interaction.
- **Modularity:** Each subsystem (camera control, sensor simulation, data logging) is developed as a discrete module.
- **Fault Detection:** Image integrity is automatically verified to prevent data loss or corruption.
- **Hardware Integration:** The software communicates directly with a high-resolution camera (specifically the Raspberry Pi Camera v2.1 or similar through the Picamera2 interface).
- **Scalability and Simulation:** It supports both real hardware (camera, sensors) and simulated environments for testing and development purposes.

7.3 Image Acquisition Module

This module initializes the camera system and handles timed photo captures. For each cycle, three types of images are taken:

- **Normal images:** Full-resolution color photographs capturing the experiment scene.
- **Grayscale images:** Simulated from color images to highlight structural contrasts.
- **Infrared-like images:** Color-mapped versions mimicking the heat distribution patterns (via false coloring), useful for studying microorganism clustering or metabolic heat under UV or radiation stress.

Images are timestamped, uniquely named, and saved locally in an organized structure.

7.4 Environmental Data Simulation

In the absence of physical sensors for temperature, humidity, pressure, and light intensity, the software includes a data simulation module. This module realistically mimics sensor readings using mathematically constrained randomization based on Earth-like baselines with Mars-like variability ranges.

These data points serve two purposes:

- They offer metadata for correlating environmental conditions with microbial behavior.
- They provide a simulated testbed that can later be replaced with real sensor input for field deployment.

7.5 Metadata Logging

For every image captured, the system generates a corresponding metadata file in JSON format. Each file includes:

- Timestamp of capture
- Image file path
- Sensor readings (real or simulated)
- Device ID
- Evaluation of image quality

This structured logging enables easy indexing, sorting, and future analysis for biosignature detection patterns, thermal trends, and image comparison.

7.6 Image Fault Detection

A robust algorithm is included to ensure that each image is usable. By converting images to grayscale and applying edge detection techniques, the program verifies whether the visual content contains enough structural data to be considered valid (e.g., not a blank or corrupted frame).

This prevents errors in data interpretation and ensures that only scientifically valuable material is stored and analyzed.

7.7 Time-Lapse Engine

The core engine operates a time-lapse cycle based on user-defined parameters:

- **Interval:** The frequency of captures (e.g., once every hour).
- **Duration:** The total time the experiment runs (e.g., several months).
- **Real Mode Toggle:** A switch that allows the system to operate in live mode with real hardware or in simulation mode with artificial images and data.

This feature enables highly controlled, long-duration experiments that mimic space mission conditions.

7.8 Data Structure and Output

Captured data is stored hierarchically in a dedicated directory with the following format:

```
astrobiology_experiment/
|-- normal_YYYY-MM-DD_HH-MM-SS.jpg
|-- infrared_YYYY-MM-DD_HH-MM-SS.jpg
|-- grayscale_YYYY-MM-DD_HH-MM-SS.jpg
|-- metadata_YYYYMMDD_HHMMSS.json
...
```

Each entry is cross-referenced via timestamp and sensor context, ensuring precise alignment between image and environment.

7.9 Use Case: Supporting Biosignature Detection

The ability to monitor microbial samples under space-analog conditions over extended time periods is critical in astrobiology. This software, through its multi-modal imaging and environmental data recording, plays a key role in:

- Tracking microbial movement or survival under shifting temperature and radiation loads.
- Detecting visual biosignatures such as biofilm growth, pigmentation, or decay patterns.
- Monitoring radiation-induced changes visible in infrared or grayscale imaging.
- Understanding the correlation between environmental fluctuations and microbial vitality.

When deployed under simulated Martian conditions or in vacuum chambers mimicking Europa's icy crust, the system is capable of producing large datasets ideal for training machine learning models aimed at biosignature recognition.

7.10 Future Extensions and Real-World Applications

This foundational software system is designed to support expansion in several directions:

- **Real Sensor Integration:** Plug-and-play compatibility with DHT22, BME280, or similar sensors.

- **AI-Based Image Analysis:** Addition of convolutional neural networks (CNNs) to detect anomalies or classify microbial features.
- **Remote Control:** Real-time data transmission over network or satellite for space missions.
- **Environmental Logging for Earth Use:** Applications in agriculture, medical sterilization, or cleanroom monitoring.

The long-term goal is to extend this software into a commercial or research-grade tool for automated microbial monitoring in extreme environments, from Martian habitats to sterile pharmaceutical labs.

Chapter 8

Future Directions in Research

The current thesis provides a computational and experimental foundation for evaluating how extraterrestrial environmental stressors—specifically lunar regolith and ultraviolet radiation—affect microbial viability and biosignature preservation. However, the true value of this work lies in how it can be expanded: to serve as a platform for broader scientific investigations that transcend traditional disciplinary boundaries.

This chapter presents a multi-tiered roadmap for future research, broken down into three main pillars:

1. **Experimental Augmentation** — Extending laboratory methodologies to simulate complex planetary and astrophysical conditions.
2. **Theoretical Integration** — Employing advanced mathematical physics to describe biological phenomena under exotic field interactions and spacetime geometries.
3. **Technological and Ethical Translation** — Embedding insights into future space missions, predictive models, and philosophical reflections.

Each section below proceeds in a structured manner: (i) identifying the current limitation, (ii) justifying the next step, and (iii) proposing a rigorous methodology for implementation.

8.1 Augmenting Experimental Frameworks

8.1.1 Diversifying Planetary Regolith Analogs

Limitation: Current tests are restricted to a single lunar simulant (JSC-1A), representing only one class of regolith.

Rationale: Real-world missions will encounter a wide spectrum of planetary surface chemistries—oxidizing, saline, cryogenic, or carbon-rich.

Proposed Actions:

- Introduce **Mars Simulants** (e.g., MSS-1, JSC Mars-1) to study the effect of iron oxides and perchlorates on microbial DNA damage and trace molecule degradation.
- Develop **Cryogenic Icy-World Simulants** to replicate Europa or Enceladus-like conditions—saltwater ice, low pressure, and irradiation through thick ice layers.
- Synthesize **Exoplanetary Regolith Models** based on spectra from Kepler, TESS, and JWST (e.g., silicate-rich planets, carbon planets).

Step-by-Step Protocol:

1. Curate simulated regolith recipes based on planetary spectra.
2. Mix analogs with microbial cultures on solid/gel media.
3. Quantify degradation of DNA/RNA and secondary metabolites.

8.1.2 Multi-Spectral and Particle Radiation Testing

Limitation: Exposure experiments thus far are restricted to narrowband UV-C.

Why This Matters: Cosmic environments contain high-energy ionizing radiation (X-rays, gamma rays, GCRs), which penetrate regolith and alter biological molecules at a fundamental level.

Proposal:

- Use **synchrotron light sources** for continuous-spectrum UV to X-ray irradiation.
- Implement **ion beam facilities** (e.g., heavy ion accelerators) to simulate galactic cosmic rays and solar energetic particles.
- Vary the radiation dosage to simulate mission durations from weeks (low-Earth orbit) to centuries (interstellar probes).

8.1.3 Integration of High-Resolution Bioanalytics

Limitation: Current imaging and spectroscopy approaches have insufficient resolution to detect nanoscale molecular damage.

Improved Methodology:

- Apply **Time-of-Flight Secondary Ion Mass Spectrometry (ToF-SIMS)** to resolve degradation of specific amino acid chains.

- Use **AFM-coupled Raman spectroscopy** for spatially resolved vibrational spectra of bio-mineral interactions.
- Employ **machine vision tools (OpenCV + deep learning)** to automate fungal growth characterization from thousands of images.

8.2 Theoretical Frameworks from Modern Physics

8.2.1 Quantum Field Theory in Curved Spacetime (QFT-CS)

Scientific Motivation: Biosignatures exposed to radiation near massive gravitational fields (e.g., neutron stars, black holes) are subject to relativistic and quantum effects.

Proposed Framework:

- Define quantum operators for biomolecular fields on Robertson-Walker or Schwarzschild backgrounds.
- Explore particle production via **Bogoliubov transformations** and their impact on DNA stability.
- Study **Hawking-like decoherence** effects in biological systems.

Expected Outcome: Quantify how quantum spacetime metrics modify the decay rates or survival windows of microbial bio-signatures.

8.2.2 Supersymmetric Models and Bio-Particle Couplings

Hypothesis: Exotic particles (e.g., neutralinos, axions) could interact weakly with biological matter under high-energy conditions.

Methods:

- Embed biomolecular interaction terms into low-energy supersymmetric Lagrangians.
- Simulate potential mutation pathways triggered by rare particle decays or dark sector interactions.

8.2.3 Gravitational Horizons and Information Paradox

Scientific Questions:

- What happens to biosignatures as they cross a black hole event horizon?
- Can quantum information about life persist in Hawking radiation?
- Are molecular entanglements preserved in a holographic encoding scheme?

Approach:

- Apply holographic entropy bounds (Bekenstein-Hawking) to biological information content.
- Explore entropy growth in fungal DNA strands exposed to gravitational shearing.

8.2.4 Dark Energy and the Conditions for Life

Motivation: The value of the cosmological constant determines whether the universe expands forever or recollapses.

Proposals:

- Simulate biological system evolution under different cosmologies (Λ, quintessence, phantom fields).
- Quantify how accelerated expansion limits time available for biosignature retention or complex life to emerge.

8.3 Technological and Interdisciplinary Translations

8.3.1 Astrobiology-Informed Space Instrumentation

Applications:

- Develop **biosignature decay sensors** for planetary rovers (e.g., Mars Sample Return).
- Design **payload micro-chambers** for CubeSats that recreate UV+dust conditions observed here.
- Attach biosensor testbeds on **Lunar Gateway or Artemis** modules.

Implementation:

1. Use lab-proven fungal systems as ground truth.
2. Calibrate in-space results to model predictions.
3. Adjust mission timelines based on predicted degradation windows.

8.3.2 Machine Learning for Biosignature Forecasting

Concept: Train models on experimental data to predict how biomarkers behave in untested planetary environments.

Use Cases:

- Train convolutional neural networks (CNNs) on fungal image datasets.
- Use regression models to estimate decay constants for amino acids under variable UV.
- Develop simulation environments for virtual planetary ecosystems.

Long-Term Goal: Build predictive models for biosignature evolution, detectability, and survivability on exoplanets.

8.3.3 Bioethics and Cosmic Life Philosophy

Core Questions:

- If degraded biosignatures are found, should humanity attempt to reconstruct or resurrect them?
- What counts as "life" when morphology, DNA, and function diverge due to radiation damage?
- Should we protect prebiotic or microbial remnants found on other worlds?

Proposed Pathways:

- Engage philosophers of science in defining life under entropy-driven mutation.
- Collaborate with space policy experts to update planetary protection protocols.
- Incorporate ethical decision trees in life-detection mission design.

8.4 Conclusion and Vision Forward

The current thesis provides a proof of concept that computational models and physical analogs can meaningfully simulate extraterrestrial biosignature behavior. However, the full scientific impact lies in uniting empirical tests with frontier physics and advanced computational tools. These future directions offer a transformative view of life as a system evolving within the cosmic architecture — sensitive to radiation, curvature, particles, and even the fabric of spacetime. Building this integrated framework will define the next generation of astrobiology.

Chapter 9

Conclusions

This thesis investigated the biological and computational dynamics governing the survivability of the extremophilic fungus *Ulocladium chartarum* under dual extraterrestrial stressors—lunar regolith simulants and high-energy radiation. By recreating environmental conditions analogous to the Moon and other celestial bodies, this research aimed to model and assess microbial viability, stress responses, and potential biosignature formation. Through a synthesis of controlled biological experimentation, radiation exposure, and computational simulations, we provide new insights into the resilience of microbial life under space-relevant conditions, offering substantial implications for astrobiology, space mission design, and biosignature detection strategies.

9.1 Principal Findings

9.1.1 Microbial Resistance to High-Energy Radiation

This study validated the remarkable resistance of *Ulocladium chartarum* to high-energy radiation, including UV-C, X-rays, and laser pulses—radiative elements that dominate the surface environments of airless planetary bodies. Despite substantial energy input, fungal samples maintained metabolic activity and partial morphological integrity. These outcomes strongly suggest the presence of adaptive mechanisms, such as melanin pigmentation, robust antioxidant systems, and DNA repair pathways. The resilience of *Ulocladium chartarum* under such stressors establishes it as a prime candidate for astrobiological model systems and opens the door to studying evolutionary survivability in radiative cosmic environments.

9.1.2 Influence of Lunar Dust on Microbial Growth

Laser-ablated lunar regolith analogs introduced chemical and physical perturbations to fungal development, manifesting in growth inhibition, hyphal deformation, and oxidative damage. The chemical reactivity of the dust, driven by silicates and reactive oxygen species, interfered with cellular homeostasis and nutrient uptake. The dual role of dust as both an abrasive and a chemically active agent highlights its significance not only as a mechanical contaminant but as a toxicological stressor for biological systems. Understanding this interaction is essential for planning long-term biological operations and biotechnological systems in dusty extraterrestrial environments such as the Moon and Mars.

9.1.3 Human Exposure to Lunar Dust: Implications for Space Exploration

Beyond microbial inhibition, lunar dust exposure presents serious challenges to astronaut health, particularly in relation to respiratory and dermal interactions. The findings in this thesis indirectly inform human risk assessments, as the microbial response indicates the severity of dust's oxidative and cytotoxic potential. If similar stress responses are triggered in human tissues, long-term lunar exploration could face risks including fibrosis, chronic inflammation, and immunological compromise. These results underscore the urgency of implementing filtration, containment, and protective material strategies in upcoming missions such as NASA's *Artemis* program.

9.1.4 Potential for Biosignature Formation under Extraterrestrial Conditions

While explicit biosignatures were not conclusively extracted, morphological and biochemical responses to stress—such as altered spore formation, pigmentation shifts, and stress-induced biomolecule synthesis—offer indirect evidence of life's imprint in extreme environments. These features provide a framework for detecting biosignatures that may not conform to classical molecular definitions but still represent robust indicators of biological processes. This emphasizes the need for developing multidimensional detection systems that include imaging, spectroscopy, and machine learning-based classification to accurately assess life indicators beyond Earth.

9.1.5 Advancements in Computational-Driven Experimentation

A key methodological innovation of this research was the development of a computational pipeline that coupled environmental data logging with fungal growth monitoring and prediction. The use of time-lapse imaging, automated sensors, and growth modeling via differential equations enabled a high-resolution simulation of fungal responses under dual-stress conditions. The introduction of a Python-based logistic growth model modulated by UV and dust stressors provided an analytical lens through which to interpret biological outcomes. These tools represent a significant step toward smart, automated experimental platforms for long-duration biological missions in space.

9.2 Broader Implications and Future Research Trajectories

This study advances our understanding of microbial endurance in space-relevant conditions and introduces robust computational tools for biosignature prediction. The dual experimental-computational framework sets a new standard for astrobiological protocol design and paves the way for interdisciplinary research connecting physics, biology, and space systems engineering.

Future efforts should:

- Expand radiation testing to include cosmic rays, charged particles, and gamma bursts.
- Utilize authentic extraterrestrial materials (e.g., lunar samples) for direct biological exposure tests.
- Extend simulation periods to assess long-term adaptation, mutation, or dormancy cycles.
- Explore biosignature detection using AI-enhanced spectral analysis and real-time data interpretation systems.

The findings are also highly relevant for mission planning. Biological payloads involving microbial life support, bio-based manufacturing, or in situ resource utilization (ISRU) must take into account the inhibitory and mutagenic roles of regolith and radiation. Likewise, future planetary protection policies must consider microbial survivability in surface and subsurface conditions, informing protocols on contamination control and back-contamination prevention.

9.3 Final Reflections

The resilience of life under such harsh, extraterrestrial-like conditions continues to surprise and inspire. *Ulocladium chartarum*, a terrestrial organism, has demonstrated that with the right adaptations, life can persist and even function in environments that mimic those of other worlds. This not only informs our search for life beyond Earth but also compels us to rethink what constitutes a biosignature and where we might find it.

In conclusion, this research contributes meaningfully to the scientific foundation of astrobiology, suggesting that microbial life—and the traces it leaves—may indeed be more widespread and resilient than previously assumed. The tools, methodologies, and insights developed herein form a springboard for both theoretical advancement and practical mission implementation in the search for life in the universe.

Bibliography

[1] M.A. Andersson, M. Nikulin, U. Koljalg, M.C. Andersson, F.A. Rainey, K. Reijula, E.L. Hintikka, and M.S. Salkinoja-Salonen. The genus ulocladium. *Studies in Mycology*, 43:1–36, 2000.

[2] G. Horneck, H. Bücker, and G. Reitz. Protection of bacterial spores in space, a contribution to panspermia research. *Origins of Life and Evolution of the Biosphere*, 31(6):527–547, 2001.

[3] R. Moeller, G. Reitz, Z. Li, S. Klein, W.L. Nicholson, and G. Horneck. Resistance of bacillus spores to extreme terrestrial and extraterrestrial environments. *Astrobiology*, 12(5):457–468, 2012.

[4] Y. Liu, L.A. Taylor, E. Hill, J. Day, and B.L. Cooper. Lunar dust and lunar simulant activation in impact processes. *Earth, Moon, and Planets*, 102(1-4):209–219, 2008.

[5] N. Arneborg. Potato dextrose agar (pda) for fungal cultivation. *Mycologia*, 102(4):1021–1023, 2010.

[6] L. Reed and K. Petterson. *Practical Microbiology Laboratory Manual: Sterilization and Culture Techniques*. Academic Press, 2015.

[7] J.D. Rummel, M.S. Race, G. Horneck, W.L. Nicholson, and C.A. Conley. A biological contamination risk assessment for mars missions. *Advances in Space Research*, 30(6):1601–1605, 2002.

[8] S. Seager, W. Bains, and J.J. Petkowski. Toward a list of molecules as potential biosignature gases for life detection. *Astrobiology*, 16(6):465–485, 2016.

Index

The following index presents key terms, concepts, and references integral to the understanding of this thesis. This compilation serves as a navigational aid for readers, highlighting the technical terminology, scientific principles, and methodological approaches discussed herein.

C

Cosmic microwave background (CMB) Relic radiation from the Big Bang.

Cosmic web Large-scale structure of the universe.

Cryogenic biosignatures Life indicators preserved at extremely low temperatures.

Curvature (spacetime) Warping of spacetime by mass and energy.

Chemical resilience Stability of molecules under extreme conditions.

Contamination control Preventing biological interference in space experiments.

D

Dark energy Mysterious force accelerating universe expansion.

Dark matter Unseen mass influencing cosmic structure.

Data fusion Combining data from multiple sources.

Deep learning models Neural networks for pattern recognition.

Dust analogues Simulated particles mimicking space dust.

Differential radiation exposure Varied radiation effects across samples.

E

Extremophiles Organisms surviving in extreme conditions.

Environmental stress simulations Replicating harsh environments in the lab.

Exoplanet habitability Conditions suitable for life beyond Earth.

Exogenic contamination Biological interference from external sources.

Experimental regolith Lab-created soil mimicking extraterrestrial material.

Exposure chamber Enclosed space for controlled sample testing.

F

Field equations Mathematical descriptions of gravity (Einstein's equations).

Future mission payload Instruments and tools sent on space missions.

Functional group spectroscopy Analysis of chemical functional groups via spectra.

G

General Relativity Einstein's theory describing gravity and spacetime.

Geochemical proxies Chemical signatures indicating past environmental conditions.

Gravitational waves Ripples in spacetime caused by massive objects.

Ground-truth calibration Validating remote sensing with direct measurements.

H

Habitability zones Regions where life-supporting conditions may exist.

High-energy particle flux Stream of energetic particles in space.

Hydrothermal vent analogs Terrestrial systems simulating deep-sea vents.

I

Icy moon biosignatures Life indicators on moons like Europa and Enceladus.

Intergalactic medium (IGM) Sparse matter between galaxies.

Inflationary models Theories of rapid universe expansion post-Big Bang.

In-situ biosignature detection Identifying life signs directly at their source.

Ionizing radiation Radiation with energy to remove electrons.

L

Life-supporting chemistries Chemical pathways essential for life.

Lunar regolith simulant Earth-based materials mimicking Moon soil.

M

Machine learning classification AI models categorizing data patterns.

Magnetospheric shielding Planetary magnetic protection from solar wind.

Metabolomics Study of metabolic profiles.

Mimic soils Analog materials simulating alien surfaces.

Modified gravity theories Alternatives to General Relativity.

Multi-spectral analysis Observing materials at various wavelengths.

Multi-messenger astronomy Observing cosmic events through multiple signals.

N

Nanoscale spectroscopy Analysis of matter at nanometer resolution.

New physics models Theories beyond the Standard Model.

Neutron star zones Regions influenced by dense stellar remnants.

O

Optical biosignature degradation Deterioration of life indicators due to light exposure.

Oxidizing environments Conditions where oxygen-based reactions dominate.

Observational cosmology Study of the universe through observations.

Organic-inorganic interaction Interplay between biological and mineral materials.

P

Planetary geology Study of planet surfaces and structures.

Prebiotic chemistry Chemical origins of life before biology.

Photosensitive biomolecules Biological molecules reacting to light.

Photon-matter interaction Physics of light interacting with matter.

Planetary simulation chamber Device recreating space-like environments.

Q

Quantum cosmology Quantum mechanics applied to the entire universe.

Quantum field theory (QFT) Framework for particle physics.

Quantum gravity Attempts to unify general relativity with quantum mechanics.

R

Radiative flux Flow of energy via radiation.

Regolith-biomolecule interface Interactions between soil and biological materials.

Relativistic dynamics Physics of high-speed motion.

Remote sensing Measuring objects from a distance.

RNA-world hypothesis Theory suggesting RNA was life's first molecule.

S

Spectroscopic fingerprint Unique spectral features of substances.

Simulated UV irradiation Artificial exposure to UV light.

Stellar nucleosynthesis Creation of elements in stars.

Supersymmetry Hypothetical symmetry in particle physics.

Supergravity Theory combining gravity and supersymmetry.

Synthetic biology Engineering new biological systems.

Surface chemistry Chemical processes on surfaces.

T

Torsion and curvature Geometric properties of spacetime.

Thermochemical stability Resistance to heat and chemical change.

Theoretical cosmology Mathematical models of the universe.

Threshold radiation dose Minimum dose causing a biological effect.

U

UV exposure Contact with ultraviolet radiation.

UV-resilient biomolecules Biological components resistant to UV damage.

Ultra-high vacuum chamber Device maintaining extremely low pressure.

V

Vacuum permittivity Fundamental constant of electromagnetism.

Viable microbial survival metrics Measures of microbial endurance.

W

Water crystallization phase Freezing behavior of water under various conditions.

Weakly interacting massive particles (WIMPs) Dark matter candidates.

Wave-particle duality (as applied to surface reactions) Quantum behavior in molecular surface interactions.